Title

Exploring the misfolding problem by systematic discovery and analysis of functional-but-degraded proteins.

Journal

Molecular Biology of the Cell, 34(13)

Authors

Lam, Breanna

Lam, Darren

Le, Tiffany

et al.

Publication Date

2023-12-01

DOI

10.1091/mbc.E23-06-0248

Peer reviewed

MBoC | ARTICLE

Exploring the "misfolding problem" by systematic discovery and analysis of functional-but-degraded proteins

Matthew P. Flagg*, Breanna Lam, Darren K. Lam, Tiffany M. Le, Andy Kao, Yousif I. Slaiwa, and Randolph Y. Hampton*

Division of Biological Sciences, the Section of Cell and Developmental Biology, University of California San Diego, La Jolla, CA 92093

ABSTRACT **In both health and disease, the ubiquitin–proteasome system (UPS) degrades point mutants that retain partial function but have decreased stability compared with their wild-type counterparts. This class of UPS substrate includes routine translational errors and numerous human disease alleles, such as the most common cause of cystic fibrosis, ΔF508-CFTR. Yet, there is no systematic way to discover novel examples of these "minimally misfolded" substrates. To address that shortcoming, we designed a genetic screen to isolate functional-but-degraded point mutants, and we used the screen to study soluble, monomeric proteins with known structures. These simple parent proteins yielded diverse substrates, allowing us to investigate the structural features, cytotoxicity, and small-molecule regulation of minimal misfolding. Our screen can support numerous lines of inquiry, and it provides broad access to a class of poorly understood but biomedically critical quality-control substrates.**

Monitoring Editor
Elizabeth Miller
MRC Laboratory of Molecular Biology

Received: Jun 27, 2023
Revised: Sep 8, 2023
Accepted: Sep 11, 2023

INTRODUCTION

As a part of protein quality control (PQC), the ubiquitin–proteasome system (UPS) selectively degrades aberrant proteins (Dikic, 2017; Jayaraj *et al.*, 2020). To do so, the UPS must identify the various misfolded species produced by environmental stress, mutations, and transcriptional and translational errors amidst a proteome of normally folded proteins. This exquisite specificity is affected by a small number of E3 ubiquitin ligases that recognize misfolded proteins and facilitate their ubiquitination, thereby targeting them to the 26S proteasome for degradation (Zheng and Shabek, 2017). PQC-substrate recognition is absolutely critical to cellular proteostasis, and defects in the UPS are a hallmark of aging as well as an expanding list of diseases referred to as proteinopathies (Klaips *et al.*, 2018).

Current mechanistic models of PQC recognition stem from extensive analysis of both PQC E3 ligases and their substrates. Studies of the latter often rely on model substrates collected from a variety of sources. One source is previously isolated point mutants that destabilize a protein and cause its degradation. Often, these substrates were identified as loss-of-function or temperature-sensitive mutants in classic forward-genetic screens: a point mutation causes PQC degradation, degradation decreases protein abundance, and decreased abundance lowers total protein function below the threshold required for cell viability (Biederer *et al.*, 1996; Gardner *et al.*, 2005; Ravid *et al.*, 2006; Farzin *et al.*, 2012). A second source is truncated versions of full-length proteins, either isolated in screens or generated by cloning. These polypeptides are unlikely to ever achieve a folded state and are often rapidly degraded (Heck *et al.*, 2010; Fredrickson *et al.*, 2011; Rosenbaum *et al.*, 2011). A third source relies on computation. A protein's crystal structure is used to predict destabilizing amino-acid substitutions *in silico*, and those

This article was published online ahead of print in MBoC in Press (http://www.molbiolcell.org/cgi/doi/10.1091/mbc.E23-06-0248) on September 20, 2023.

Conflicts of interest: The authors have declared that no conflict of interest exists.

Author contributions: These studies were conceptualized and designed by R.Y.H. and M.P.F. Screening of Ade1 and Aro7 was performed by B.L. and M.P.F. Screening of Lys1 was performed by Y.I.M., A.K., and M.P.F. All CHX chases and all Western blotting were performed by M.P.F. Aro7 dose–response experiments were performed by T.M.L. and B.L. Microscopy was performed by M.P.F. and T.M.L. Yeast serial dilution assays and Targeted Ubiquitin System 2.1 screening were performed by D.K.L. and M.P.F. The manuscript was written by M.P.F. and edited by R.Y.H., M.P.F., and T.M.L.

*Address correspondence to: Randolph Y. Hampton (rhampton@ucsd.edu); Matthew P. Flagg (mflagg@ucsd.edu).

Abbreviations used: CHX, cycloheximide; GFP, green fluorescent protein; PQC, protein quality control; Trp, tryptophan; Tyr, tyrosine; UPS, ubiquitin–proteasome system; WT, wild type; YRC, yeast recombination cloning.

substitutions are then tested for UPS-mediated degradation in vivo (Nielsen *et al.*, 2017; Abildgaard *et al.*, 2019). Finally, a variant of PQC substrates are naturally degraded proteins. These appear to display structural features of quality control as part of cellular regulation of their abundance (Hampton *et al.*, 1996; Swanson *et al.*, 2001; Foresti *et al.*, 2013; Foresti *et al.*, 2014; Khmelinskii *et al.*, 2014; Zelcer *et al.*, 2014; Wangeline *et al.*, 2017; Wangeline and Hampton, 2021). These diverse model substrates have supported in-depth studies of key and conserved PQC ligases, but small collections of structurally disparate substrates are not sufficient to define biologically relevant misfolding.

To create more comprehensive substrate collections, investigators have developed and refined a number of screening and genetic approaches. For instance, several groups have designed screens to discover "degrons," short amino-acid sequences that confer degradation upon a reporter protein (Gilon *et al.*, 2000; Geffen *et al.* 2016; Maurer *et al.*, 2016). In a recent example of this approach, a high-throughput selection was used to isolate degrons that lowered cytosolic reporter-protein abundance. This method uncovered 130 degrons targeted by the PQC E3 ligase Doa10, 13 of which were derived from segments of native proteins (Geffen *et al.*, 2016). Analysis of that substrate collection and others like it have indicated some structural features recognized by PQC ligases. These include amphipathic helices in the case of Doa10 and its mammalian homologue MARCH6 (Johnson et al, 1998; Geffen *et al.*, 2016; Chua *et al.*, 2017) and hydrophobicity and disorder in the case of the PQC E3 ligase San1 (Fredrickson *et al.*, 2011; Rosenbaum *et al.*, 2011; Fredrickson *et al.*, 2013). The field has begun to define the biochemical basis of substrate recognition by employing in-depth screening and well-characterized substrate collections.

However, a systematic, screen-driven approach has yet to be applied to a biomedically and biologically critical subset of degraded point mutants: minimally misfolded proteins. We categorize a protein as minimally misfolded when a single destabilizing mutation causes PQC degradation but does not ablate protein function. Minimal misfolding can have important clinical outcomes stemming from both degradation and proteotoxic stress. The most famous cases are the cystic fibrosis variant ΔF508-CFTR and the sickle cell anemia variant HbS D6V (Ingram, 1957; Harrington *et al.*, 1997; Guerriero and Brodsky, 2012), but it is possible that minimal misfolding underlies a swath of human diseases. Studies combining clinical and computational data suggest that the majority of monogenic diseases are caused by mutations that destabilize protein structure, often by a ΔΔG of as little as 1–3 kcal mol^{-1} (Yue *et al.*, 2005; Redler *et al.*, 2016), and high-throughput in vivo approaches corroborate that such mutations lower protein abundance (Matreyek *et al.*, 2018; Cagiada *et al.*, 2021; Jia *et al.*, 2021). When examined individually in vivo, many disease-associated mutations are degraded by the UPS but nonetheless retain partial function (Nielsen *et al.*, 2017; Abildgaard *et al.*, 2019; Gersing *et al.*, 2021).

Minimally misfolded proteins are also naturally produced during transcription and translation. A recent study in *Escherichia coli* demonstrates that amino-acid misincorporations occur at frequencies as high as 1 in 1000 residues, and the resultant substitutions cause an average ΔΔG of 1.45 kcal mol^{-1} (Garofalo *et al.*, 2019; Mordret *et al.*, 2019). Insights from both disease states and normal biology imply that minimally misfolded point mutants are a large and highly relevant class of quality-control substrate that justifies more encompassing study.

We therefore devised a screen for point mutations that cause a stable protein to become minimally misfolded. We sought to create simple models of translational errors and disease-causing mutants, and we hoped to contextualize screen-isolated substitutions with solved x-ray crystal structures. By inferring the destabilizing effects of different point mutations, we aimed to connect minimal structural insults to the specific PQC pathways that recognize them.

To further investigate the features of minimal misfolding, we screened a simple allosteric protein, chorismate mutase (CM), and tested if the stability of degraded CM variants could be regulated by the protein's allosteric effectors. Classically, orthosteric and allosteric ligands have been shown to facilitate integral cell-membrane protein folding and maturation (Morello *et al.*, 2000; Bernier *et al.*, 2004a; Bernier *et al.*, 2004b; Leidenheimer and Ryder, 2014). Such ligands are referred to as pharmacological chaperones or correctors, and they compose one part of a multidrug treatment for cystic fibrosis (Pike *et al.*, 2001; Van Goor *et al.*, 2009; Van Goor *et al.*, 2011; Rowe and Verkman, 2013; Cornella-Taracido and Garcia-Echeverria, 2020; Pedemonte *et al.*, 2020). Ligand binding can also cause targeted misfolding. For instance, the yeast HMG-CoA reductase isozyme Hmg2 is subject to UPS-mediated degradation when a sterol pathway metabolite binds to it and causes it to undergo reversible misfolding (Shearer and Hampton, 2005; Garza *et al.*, 2009; Wangeline and Hampton, 2018). We have named this mode of degradative feedback regulation "mallostery" due to its many similarities to classic allosteric regulation (Wangeline and Hampton, 2018). Ligand-dependent degradation imposes feedback regulation in a number of other circumstances (Zhu and Wojcikiewicz, 2000; Song *et al.*, 2005; Howe *et al.*, 2015; Skieterska *et al.*, 2017; van den Boomen *et al.*, 2020), and small molecules that bind to a target protein and cause misfolding represent a promising but underutilized therapeutic approach (Cornella-Taracido and Garcia-Echeverria, 2020). Such ligands are referred to as "monovalent degraders" (in contrast to bivalent PROteolysis TArgeting Chimeras [PROTACs], which do not cause protein misfolding but rather recruit UPS machinery to a target protein; Sun *et al.*, 2019; Cornella-Taracido and Garcia-Echeverria, 2020). We explored whether misfolded CM variants were subject to either mode of ligand-regulated quality-control degradation.

Overall, our genetic approach systematically generates examples of an understudied but pervasive class of quality-control substrate. The screen is broadly applicable, but by focusing on minimally misfolded variants of simple proteins, we were able to reveal the extraordinary complexity of the quality-control code that lurks in even one domain of a monomeric, globular protein.

RESULTS

An optical screen for minimally misfolded point mutants

Degraded point mutants have reduced steady-state abundance compared with the stable, wild-type protein. This phenotype can be observed using GFP-tagged substrates and yeast-colony fluorescence: colonies expressing degraded mutants are dim, whereas colonies expressing stable mutants or the wild-type protein are bright. We used this feature of PQC degradation in a primary screen for novel substrates.

To create mutant-expressing yeast colonies, genes of interest were mutagenized with error-prone polymerase chain reaction (PCR) (Agilent), and the resultant amplicons were used for yeast recombination cloning (YRC; Supplemental Figure S1A). YRC yielded GFP-tagged mutants and thousands of fluorescent colonies that each bore a unique, plasmid-born mutant (Muhlrad *et al.*, 1992). Dim colonies bearing putative substrates were identified with a simple GFP-visualizing setup: a halogen bulb and a narrow band-pass filter created a source of GFP-exciting blue light; goggles with a long-pass filter blocked background light and allowed GFP fluorescence to be scored (Cronin and Hampton, 1999).

While this primary screen eliminated many stable mutants, dim candidates included mutations that lowered colony fluorescence in ways unrelated to degradation (unpublished data). Other screens for PQC substrates have encountered similar pitfalls. Geffen *et al.* (2016) report degrons that significantly lowered reporter protein abundance but did not cause UPS-mediated degradation. Other indicators of putative PQC degradation, such as temperature-sensitive growth, can also yield stable mutants (Farzin *et al.*, 2012).

We therefore developed a secondary screen for candidates made dim by UPS-mediated degradation. Specifically, we employed a plate-based assay for dim candidates that become bright when proteasome activity is compromised. This was facilitated by a hypomorphic *RPN1*/*HRD2* allele of the 26S proteasome, *hrd2-1*, which markedly stabilizes a broad range of quality control substrates (Hampton *et al.*, 1996; Wilhovsky *et al.*, 2000; Murray and Correia, 2001). The *hrd2-1* allele is particularly useful for screening due to its lack of strong growth defects.

To directly test candidates for stabilization in *hrd2-1* strains, we used a yeast counterselection strategy. The primary screen for dim colonies was performed in a *hrd2-1* strain bearing a *CEN/ARS URA3-HRD2* plasmid, which fully complemented the *hrd2-1* mutant. Once dim colonies were isolated, the *HRD2* plasmid was removed by counterselection of the *URA3* marker. This was achieved by plating candidates on medium with 5-FOA, which only allows growth of cells that have lost the *URA3-HRD2* plasmid. Counterselection thereby imposed 26S-proteasome deficiency in the plasmid-cleared colonies (Supplemental Figure S1B). In this uncovered *hrd2-1* background, markedly increased fluorescence indicated a PQC substrate (Supplemental Figure S1C).

Next, *HRD2* strains bearing putative substrates were directly tested for degradation by cycloheximide (CHX) chase using a flow cytometer (Supplemental Figure S1D). Mutant plasmids encoding unstable variants were then isolated and sequenced. Together, the primary and secondary screens typically identified two to five substrates from ~1000 colonies. In each case below, the screen was repeated until it produced consensus mutants, a saturation benchmark usually attained after screening ~20,000 colonies in the case of a ~1-kb gene.

The screen can isolate any mutation that causes PQC degradation, but we sought to carefully constrain it and to collect solely minimally misfolded point mutants. To do so, we searched protein databases for soluble, monomeric proteins with easy-to-score functions and solved x-ray crystal structures. These criteria allowed us to preclude many other causes of PQC degradation, such as nonsense mutations that produce nonfunctional truncations and amino-acid substitutions that prevent multimerization, thereby unmasking a degradation signal without destabilizing tertiary structure (Juszkiewicz and Hegde, 2018; Padovani *et al.*, 2022; Pla-Prats and Thomä, 2022; Yagita *et al.*, 2023). The following screens produced only full-length, functional-but-degraded mutants. We hoped that these subtle structural perturbations would justify reference to solved crystal structures, allowing us to map substitutions and to discern "rules" of minimal misfolding.

Screening of *ADE1* produces minimally misfolded UPS substrates

The first parent protein we examined was N-succinyl-5-aminoimidazole-4-carboxamide ribotide synthetase (Ade1). Ade1 is a stable (Supplemental Figure S2), cytosolic monomer with a two-domain structure revealed by crystallography (Levdikov *et al.*, 1998; Huh *et al.*, 2003). Ade1 catalyzes an intermediate step of adenine biosynthesis, thus *ade1*Δ nulls cannot grow on plates lacking adenine (Roman, 1956). This nutritional requirement facilitated a simple readout of Ade1-mutant function: when expressed in an *ade1*Δ null, functional Ade1 mutants support growth on plates lacking adenine. Ade1-GFP was stable, and fully complimented *ade1*Δ nulls (Supplemental Figure S3), allowing us to assess both optics and function while screening.

We mutagenized the *ADE1* open-reading frame (ORF) and performed YRC in an *ade1*Δ-null version of the screening strain described above. To assess the quality and coverage of the mutagenesis, we transformed onto plates with adenine, picked 50 colonies at random, and recovered plasmids from each. Sequencing confirmed a desired low rate of mutagenesis (0.6 mutations per mutant recovered) that facilitated isolation of point mutants from the screen (Supplemental Table S1). Randomly selected mutants were distributed throughout the *ADE1* ORF, as observed in other analyses of the Mutazyme II kit (Wong *et al.*, 2006).

Having confirmed the quality of our library, we screened ~20,000 colonies grown on plates with adenine. Dim colonies were isolated then incubated on plates lacking adenine at a permissive temperature. Mutants that supported growth were preliminarily scored as functional, and these were screened for UPS-dependent degradation. Roughly 40 candidates retained function, increased in fluorescence after *HRD2* counterselection, and underwent degradation in a preliminary CHX chase. In total, we isolated nine destabilizing point mutations at six distinct residues, and we recovered most mutants on multiple occasions, indicating that we approached or achieved screen saturation (Supplemental Table S2).

We converted the plasmids recovered from the screen into stable, chromosome-integrating plasmids using an integrating-after-*CEN*-excision approach (Flagg *et al.*, 2019). The resultant plasmids were then transformed as single integrants into standard lab strains to confirm that each mutant was a minimally misfolded PQC substrate. First, we retested function by expressing mutants in an *ade1*Δ null. Each supported growth on plates lacking adenine (Supplemental Figure S3). We then tested for UPS-mediated degradation using CHX chase in the presence or absence of the proteasome inhibitor MG132. MG132 stabilized all mutants, confirming proteasome dependence as well as the efficacy of the secondary screen (Supplemental Figure S4). CHX chase also demonstrated the breadth of degradation rates detected by our optical screen: substrate half-lives ranged from roughly 30 min to over 5.5 h.

As an additional, independent test for minimal misfolding, we subjected each Ade1 mutant to in vivo treatment with glycerol, a chemical chaperone. Chemical chaperones favor protein folding and stabilize misfolded substrates in vivo (Shearer and Hampton, 2004; Zhao *et al.*, 2013; Auton and Bolen, 2015). By contrast, chemical chaperones have no effect on proteins that are grossly misfolded or unfolded, such as the severely misfolded 6myc-Hmg2 and the nonfolding carboxypeptidase Y mutant CPY* (Shearer and Hampton *et al.*, 2004). All Ade1 mutants were stabilized in the presence of glycerol (Supplemental Figure S5).

Because they met our criteria for minimal misfolding, Ade1 substitutions were located in the solved crystal structure and their destabilizing effects were inferred. Using three-dimensional structures in this way has indicated the effects of many disease-causing mutations. The majority lead to canonical disruptions of a protein's native structure, ranging from cavity formation to backbone strain (Wang and Moult, 2001; Yue *et al.*, 2005; Redler *et al.*, 2016). High-throughput approaches have led to similar findings. Roughly a thousand variants that lowered PTEN steady-state levels were mapped to the protein's crystal structure, and lowered abundance could often be explained by the disruption of a hydrophobic pocket or the loss of intradomain polar contacts (Matreyek *et al.*, 2018).

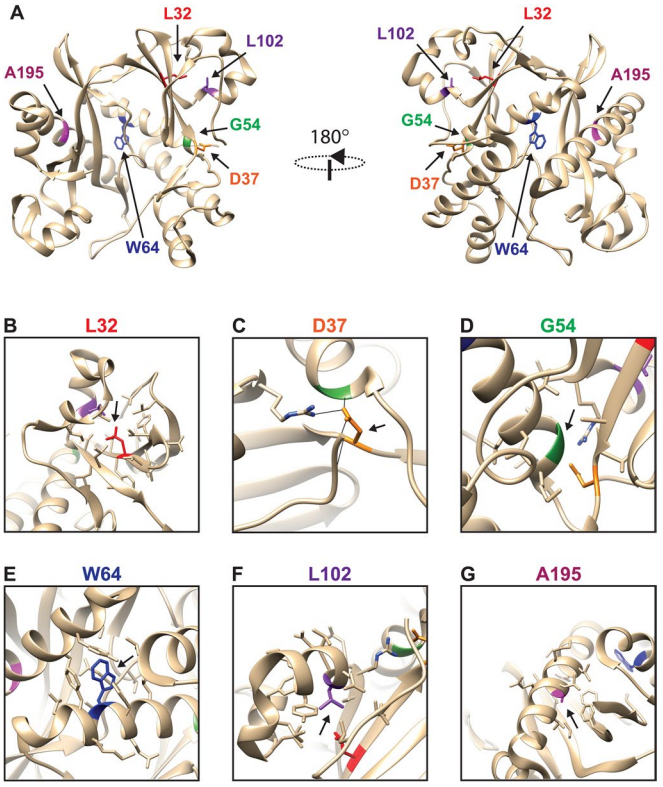

FIGURE 1: The position of minimally misfolded mutants in the Ade1 structure. (A) Two perspectives of the Ade1 crystal structure (PDB 1A48). Arrows and color-coded sidechains indicate positions at which destabilizing mutations were isolated. (B–G) Closeups of positions at which destabilizing substitutions were isolated. In each inset, the position's wild-type amino acid is shown, color coded, and indicated by an arrow. To demonstrate proximity and spatial relationships, additional screen-isolated residues that fall within an inset's field of view are shown and color coded as in A. In the case of buried positions (A and D–G), additional amino acids that fall within a 5 Å zone are shown in khaki. In the case of intramolecular hydrogen bonding (B), black lines show hydrogen bonds predicted by UCSF Chimera under relaxed constraints.

The destabilized Ade1 point mutants isolated by our screen caused similar perturbations (Figure 1; PDB 1A48; Pettersen *et al.*, 2004). The majority of substitutions introduced charge or polarity into the interior of the native structure (Ade1-L32R, G54E, G54R, W64R, A195D; Figure 1, B, D, E, G). The variant Ade1-D37V abrogated several intradomain polar interactions: the carboxylic acid of the original aspartic acid forms hydrogen bonds with both R105 and the peptide backbone at position 54 (Figure 1C). This latter hydrogen bond may be disrupted by the screen-isolated substitution Ade1-G54V (Figure 1D), which caused numerous steric clashes with the peptide backbone at T26 and D37. Finally, two mutations introduced prolines into secondary structures, one on an α helix (Ade1-L102P; Figure 1F) and one on a β strand in a β sheet (L32P; Figure 1B). In sum, each Ade1 mutant exhibited both canonically disrupted protein folding and intact enzymatic function.

A San1–Doa10 pathway degrades all Ade1 mutants

Structural analysis revealed that different Ade1 mutants disrupted a variety of secondary structures and hydrophobic pockets throughout the protein (Figure 1A). We wondered if a common PQC pathway would degrade each, or if different pathways would degrade different variants, perhaps according to their distinct structural and biochemical properties. To discern between those possibilities, we set out to identify the PQC pathway(s) that degraded each mutant using direct genetic analysis.

In *Saccharomyces cerevisiae*, the major E3 ligases that mediate cytosolic PQC are the soluble E3 ligase Ubr1, the ER-transmembrane ligase Doa10, and the nuclear ligase San1. These E3s are often functionally redundant, especially San1 and Ubr1, which almost always act in parallel (Eisele and Wolf, 2008; Heck *et al.*, 2010; Nillegoda *et al.*, 2010). However, it is also well-documented that individual PQC ligases can recognize distinct degrons that other ligases cannot (Swanson *et al.*, 2001; Geffen *et al.*, 2016). A cytosolic substrate may be recognized by one, two, or all three ligases depending on the PQC determinants displayed upon misfolding (Heck *et al.*, 2010; Breckel and Hochstrasser, 2021; Hickey *et al.*, 2021).

We assayed each Ade1 variant for Doa10-, San1-, and Ubr1-dependent degradation using CHX chase in *doa10Δ, san1Δ, ubr1Δ*, and combined null backgrounds. San1 mediated the majority of the degradation of each mutant, and in every case, a *doa10Δsan1Δ* null led to strong but incomplete stabilization (Figure 2). The absence of Ubr1 had no discernable stabilizing effect on any of the variants (Supplemental Figure S6), and stability was not enhanced in the *san1Δubr1Δdoa10Δ* null (Supplemental Figure S7).

We therefore concluded that destabilizing substitutions in distinct regions of the Ade1 structure were uniformly subject to a San1-Doa10–mediated quality control pathway. Taken alone, these data would imply that all destabilized variants of a protein are recognized and degraded by the same PQC pathway, even when they cause a variety of structural disruptions. We wondered if this was a general feature of minimal misfolding.

Distinct PQC pathways degrade spatially grouped Lys1 mutants

To expand our analysis, we screened a second protein, saccharopine dehydrogenase (Lys1). Like Ade1, Lys1 is a two-domain, soluble, monomeric protein with a solved crystal structure (Burk *et al.*, 2007). A minor drawback of Lys1, its native localization to the peroxisome, is easily overcome by a C-terminal GFP fusion. GFP blocks the protein's peroxisomal localization sequence, thereby rendering Lys1-GFP a stable (Supplemental Figure S8) and functional cytosolic protein (Al-Saryi *et al.*, 2017). Lys1 catalyzes the final step of lysine biosynthesis, and *lys1Δ* nulls cannot grow on plates lacking lysine (Jones and Broquist, 1965). The wild-type cytosolic GFP fusion rescues this nutritional phenotype, allowing mutant function to be scored by lysine prototrophy (Supplemental Figure S9; Hawthorne and Mortimer, 1960; Saunders and Broquist, 1966).

We screened ~20,000 colonies expressing mutated Lys1-GFP and isolated eight destabilizing point mutations at seven distinct residues. Each mutant complemented the *lys1Δ* null, although some required *CEN/ARS* plasmids to achieve adequate protein steady-state levels (Supplemental Figure S9). Each mutant was also stabilized by proteasome inhibitor (Supplemental Figure S10, A–B and D) and by the chemical chaperone glycerol (Supplemental Figure S11). The Lys1 screen isolated novel, minimally misfolded point mutants.

We therefore used the wild-type Lys1 crystal structure to infer the effect of each point mutation (Figure 3; PDB 2Q99). Mutations introduced charge or polarity into hydrophobic pockets of the protein (Lys1-V26D, W151R, P194Q, I254N, W353R; Figure 3, A and B and E–H) or interfered with secondary structures (Lys1-L29P, L146P, W151G; Figure 3, C–E). Again, amino-acid substitutions isolated by the screen destabilized canonical features of globular protein structure.

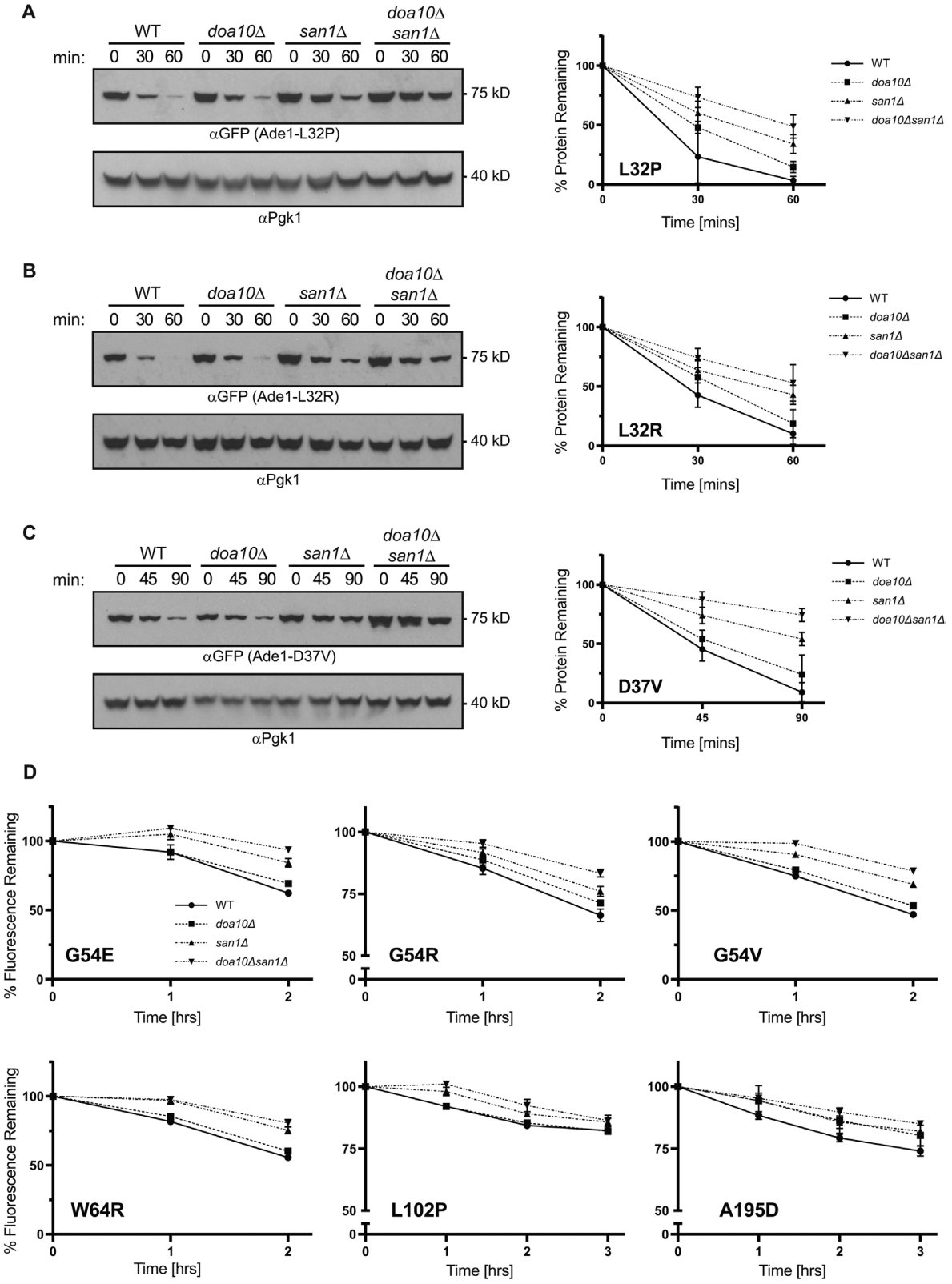

FIGURE 2: Ade1 mutants are degraded by San1 and Doa10 in parallel. (A–C) WT, *san1*Δ, *doa10*Δ, and *san1*Δ*doa10*Δ null strains expressing Ade1-L32P (A), L32R (B), or D37V (C) were grown into log phase and treated with CHX. At the indicated timepoints, cells were harvested and lysed. Lysates were then Western blotted using α-GFP and α-Pgk1. Densitometry was performed with FIJI. Each α-GFP band was normalized to its corresponding α-Pgk1 band, and Pgk1-normalized readings were normalized to t = 0. Graphs show the mean and SD of three experiments. (D) WT, *san1*Δ, *doa10*Δ, and *san1*Δ*doa10*Δ–null strains expressing Ade1-G54E, G54R, G54V, W64R, L102P, or A195D were grown into log phase and treated with CHX. At the indicated timepoints, 10,000 cells were analyzed by flow cytometry. Reads are normalized to *t* = 0, and graphs show mean and SD from three experiments.

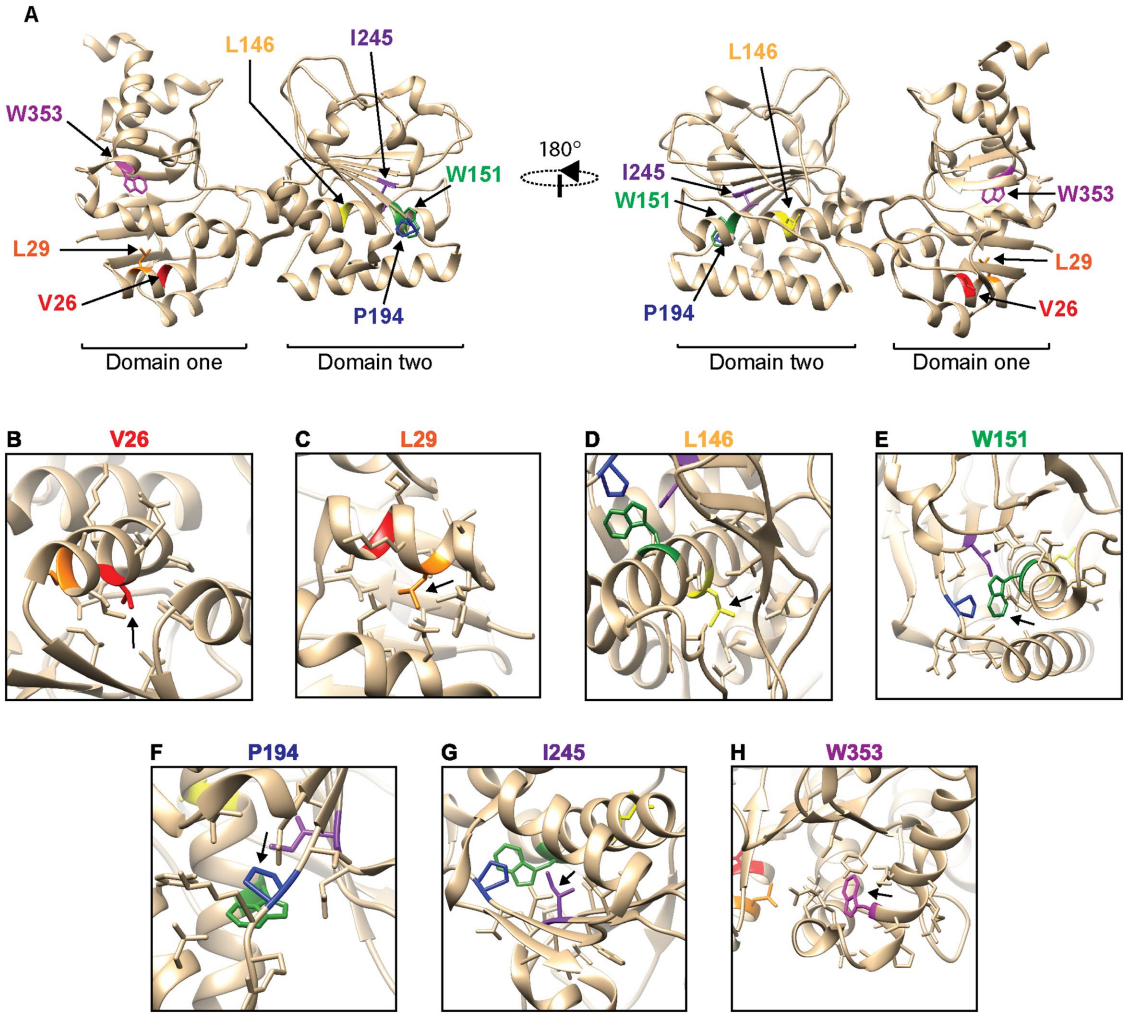

FIGURE 3: The position of minimally misfolded mutants in the Lys1 Structure. (A) Two perspectives of the Lys1 crystal structure (PDB 2QRL). Arrows and color-coded sidechains indicate positions at which destabilizing mutations were isolated. (B–H) Closeups of positions at which destabilizing substitutions were isolated. In each inset, the position's wild-type amino acid is shown, color coded, and indicated by an arrow. To demonstrate proximity and spatial relationships, additional screen-isolated residues that fall within an inset's field of view are shown and color coded as in A. In each case, additional amino acids that fall within a 5 Å zone are shown in khaki.

We noticed that substitutions formed clusters in the Lys1 3D structure. Lys1-W151R, P194Q, and I254N are within five angstroms of one another and constitute a hydrophobic pocket in the second domain (Figure 3, A and E–G). While it does not occupy this pocket, Lys1-L146P (Figure 3D) is on the same α-helix as Lys1-W151R. A similar grouping in the first domain is composed of Lys1-L29P and V26D (Figure 3, A–C). Both of those substitutions occur on the same α-helix. A final variant, Lys1-W353R, is somewhat more isolated. The first domain of Lys1 contains the protein's N and C terminus. Lys1-L29 and V26 are on the first, C-terminal α-helix of the protein, whereas Lys1-W353 is on the final, N-terminal helix (Figure 3H). Nevertheless, the Chimera distance tool estimates that the closest atoms of the Lys1-W353 and L29 sidechains are separated by only nine angstroms (Pettersen *et al.*, 2004).

To determine the PQC pathway(s) involved in degradation, we first tested grouped mutants in the second domain (Lys1-W151G, W151R, P194Q, I254N, and L146P) using single and multiple ligase nulls, as above. CHX chase showed that all five mutants were partially stabilized in *san1*Δ and *ubr1*Δ null backgrounds and fully stabilized in a *san1*Δ*ubr1*Δ null (Figure 4, A and B; Supplemental Figure S12A). Those data were consistent with measurements of mutant steady-state levels in each background. Flow cytometry showed a moderate increase in mutant steady-state levels in *san1*Δ and *ubr1*Δ null backgrounds and a marked increase in the *san1*Δ*ubr1*Δ null (Supplemental Figure S12B). Like our Ade1 mutants, this cluster of substitutions led to one PQC outcome but, notably, by a Ubr1-dependent pathway distinct from the Ubr1-independent pathway of Ade1 substrates.

To determine if this San1-Ubr1 pathway degraded all Lys1 mutants, the domain-one mutants Lys1-V26D and L29P were expressed in wild-type and *san1*Δ*ubr1*Δ null backgrounds. In contrast to the mutants in domain two, neither substrate was stabilized by the absence of San1 and Ubr1 (Figure 4, C and D). We wondered if the Lys1 crystal structure could be used to predict an additional mutant that would cause San1-Ubr1-indendent degradation. Lys1-V26 contributes to the same hydrophobic pocket as Lys1-I36 (Figure 4E). We therefore used site-directed mutagenesis to create *lys1-I36D*. Like Lys1-V26D and L29P, I36D caused proteasome-dependent (Supplemental Figure S10C) and San1-Ubr1-independent degradation (Figure 4F). Unlike the case of Ade1, Lys1 mutants led to different

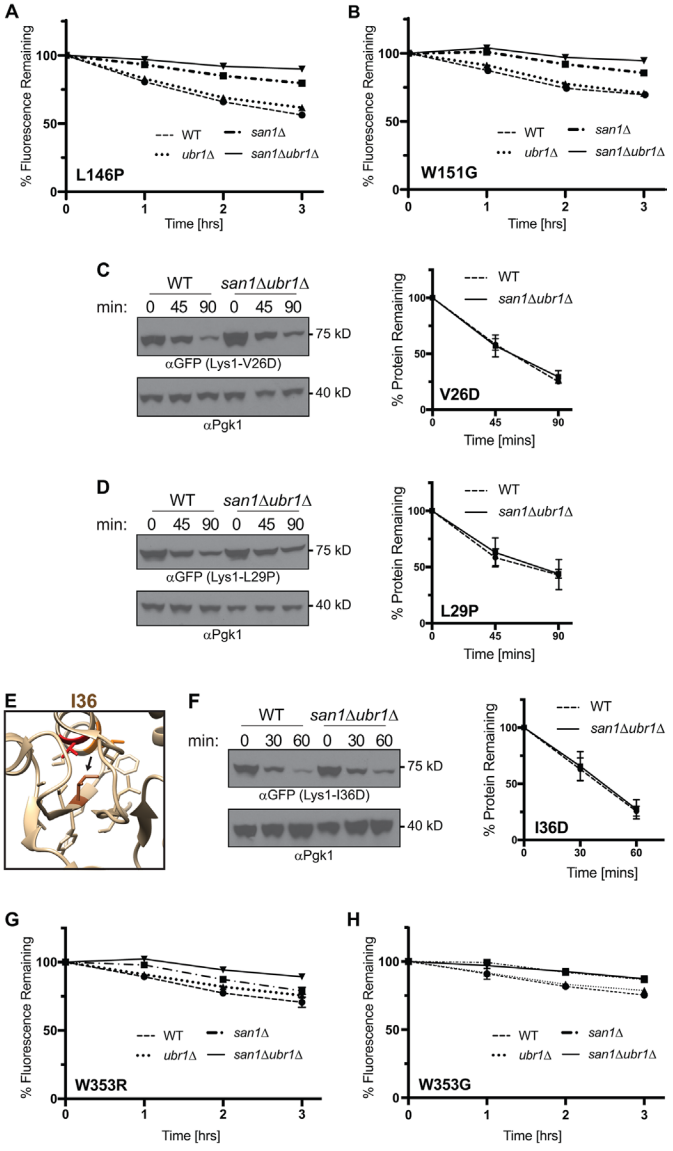

FIGURE 4: Grouped Lys1 mutants are degraded by distinct PQC pathways. (A–B) Degradation of Lys1-L146P and W151G is San1 and Ubr1 dependent. WT, *san1*Δ, *ubr1*Δ, and *san1*Δ*ubr1*Δ null strains expressing Lys1-L146P (A) or W151G (B) were treated with CHX, and 10,000 cells were analyzed by flow cytometry at the timepoints indicated. The mean and SD of three experiments are shown. (C–D) Degradation of Lys1-V26D and L29P is San1 and Ubr1 independent. WT and *san1*Δ*ubr1*Δ strains expressing Lys1-V26D (C) and L29P (D) were treated with CHX and lysed at the times indicated. Lysates were then Western blotted using α-GFP and α-Pgk1. The mean and SD of three experiments are shown. (E) Position of I36 in the Lys1 crystal structure (PDB 2QRL). The wild-type isoleucine is shown, color coded, and indicated by an arrow. Amino acids within a 5 Å zone of I36 are shown, including V26 (red) and L29 (orange). (F) Degradation of Lys1-I36D is San1 and Ubr1 independent. WT and *san1*Δ*ubr1*Δ null strains expressing Lys1-I36D were subjected to CHX chase and Western blotting, as described above. The mean and SD of three experiments are shown. (H–I) Degradation of Lys1-W353R and W353G is San1 and Ubr1 dependent. WT, *san1*Δ, *ubr1*Δ, and *san1*Δ*ubr1*Δ null strains expressing Lys1-W353R (G) or W353G (H) were subjected to CHX chase and flow cytometry, as described above. The mean and SD of three experiments are shown.

PQC outcomes depending on their location in the wild-type structure.

To determine if all domain-one mutants were subject to San-Ubr1-independent degradation, we introduced the remaining domain-one mutant, Lys1-W353R, into *san1*Δ, *ubr1*Δ, *san1*Δ*ubr1*Δ null backgrounds and tested stability by CHX chase. In contrast to the other mutations in domain one, Lys1-W353R was partially stabilized in *san1*Δ and *ubr1*Δ nulls and fully stabilized in a *san1*Δ*ubr1*Δ null (Figure 4G). To further support this finding, we used site-directed mutagenesis to create *lys1-W353G*. Lys1-W353G was also fully stabilized in a *san1*Δ*ubr1*Δ null (Figure 4H). Thus, even within one domain of a monomeric protein, different substitutions can cause degradation by different PQC pathways.

Unveiling Hul5 involvement in proteolysis of Lys1 variants

Lys1-V26D, L29P, and I36D seemed to be recognized by an unidentified PQC E3 ligase or ligases. To explore this possibility, we used the Targeted Ubiquitin System (TUS; Hickey *et al.*, 2021). This collection of yeast strains includes single nulls of each of the nonessential E3 ubiquitin ligases as well as several nonessential Fbox proteins. We transformed Lys1-V26D-GFP into each null and subjected the resultant strains to flow cytometry.

Using increased steady-state fluorescence as an indicator of stabilization, we identified the *hul5*Δ null as the only strongly stabilizing background (Supplemental Figure S13; Supplemental Table S3). In a previous study, Hul5 was identified as a major mediator of protein degradation after heat shock, supporting the possibility that the ligase recognized and ubiquitinated our Lys1 substrates (Fang *et al.*, 2011). The second largest increase in steady-state levels was observed in a *dia2*Δ null background. This strain has been isolated in similar screens as a null that increases substrate transcription, and it was scored as a false positive (Hickey *et al.*, 2021). We therefore investigated the role of the E4/E3 ligase Hul5 in the degradation of our San1-Ubr1-independent Lys1 substrates.

In the process of confirming the *hul5*Δ null phenotype, we experienced a technical difficulty in complimenting the *hul5*Δ null strain with a *CEN/ARS* plasmid. Our *HUL5-URA3-CEN* plasmid was sequenced and contained the ORF as well as ~500 bp upstream and downstream of the gene; it provided the appropriate uracil prototrophy upon transformation; and a PCR test (using one primer on the plasmid backbone and one primer on the *HUL5* gene) confirmed the presence of the plasmid in the resultant strain (unpublished data). Nevertheless, there was no apparent change in phenotype as scored by fluorescence (unpublished data). In the following data, we used a *hul5*Δ*::URA3* null and successfully complimented this strain by integrating a *HUL5* fragment at the endogenous locus (using a 5-FOA counterselection). While some have succeeded in complimenting a *hul5*Δ null with a *CEN* plasmid, we caution others who intend to use this common yeast-genetics approach. Anecdotal evidence suggests that the *HUL5* fragment typically cloned into yeast shuttle vectors may have a cryptic centromeric sequence that precludes stable complementation when part of a *CEN/ARS* plasmid (T. Mayor; personal communication).

We directly analyzed Lys1-V26D, L29P, and I36D degradation in a *hul5*Δ null background using CHX chase. In preliminary testing, we performed chases using a flow cytometer. We found that all three substrates were completely stabilized in a *hul5*Δ null and that *HUL5* complementation restored wild-type degradation (Figure 5A; Supplemental Figure S14A). We attempted to confirm this result using immunoblotting. To our surprise, the blots showed relatively minor

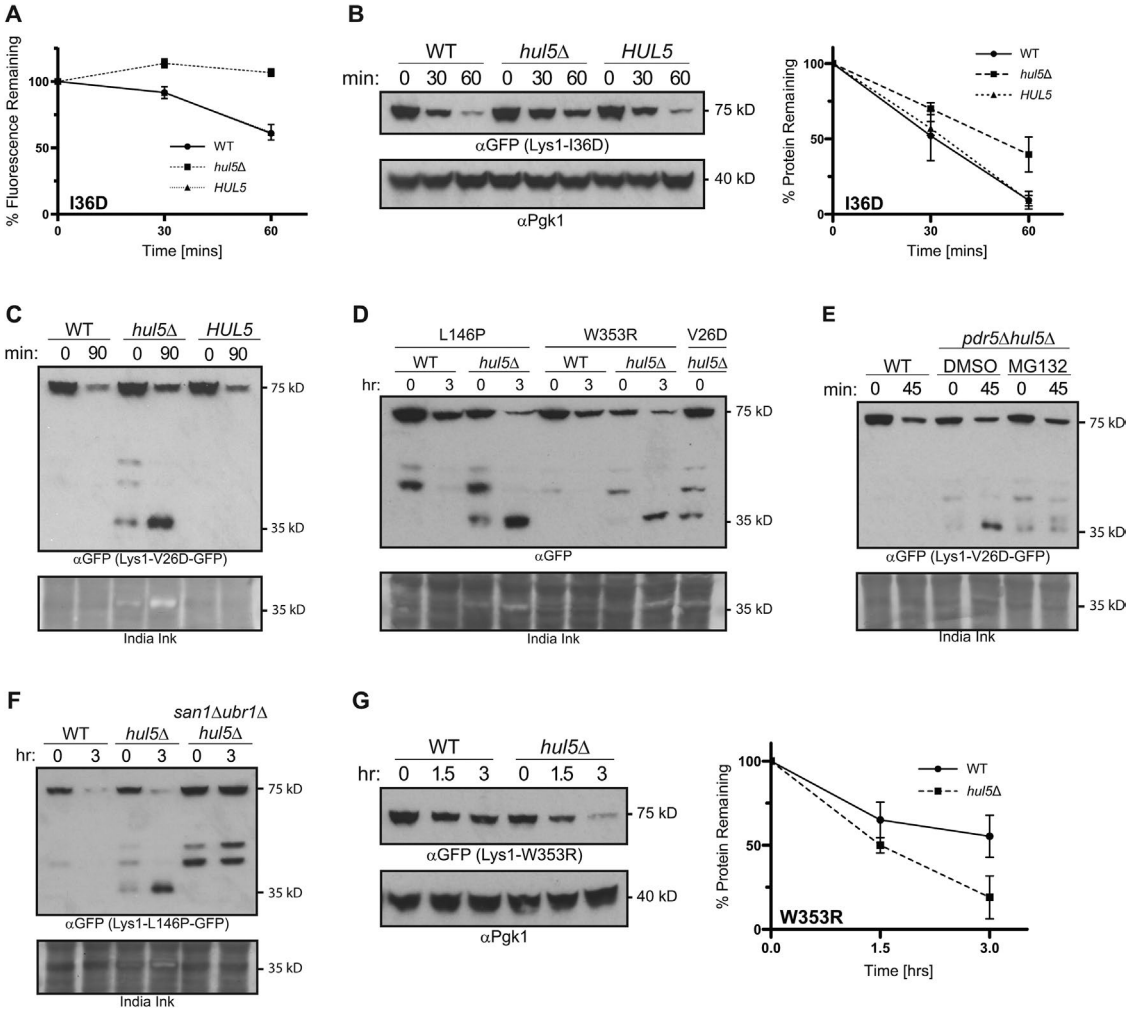

FIGURE 5: Common and contrasting effects of Hul5 on the proteolysis of Lys1 mutants. (A) Flow-cytometer CHX chase suggests that Lys1-I36D is stable in a *hul5*Δ null background. WT, *hul5*Δ null, and *HUL5*-complimented strains expressing Lys1-I36D were treated with CHX, and 10,000 cells were analyzed by flow cytometry at the timepoints indicated. The mean and SD of three experiments are shown. (B) Western blot CHX chase demonstrates that Lys1-I36D is partially stabilized in a *hul5*Δ null background. WT, *hul5*Δ null, and *HUL5*-complimented strains expressing Lys1-I36D were treated with CHX and lysed at the times indicated. Lysates were then Western blotted using α-GFP and α-Pgk1. The mean and SD of three experiments are shown. (C–D) Lys1 mutants form a ~37 kDa fragment in a *hul5*Δ null background. (C) WT, *hul5*Δ null, and *HUL5*-complimented strains expressing Lys1-V26D were treated with CHX and lysed at the indicated times. Lysates were then Western blotted using α-GFP (top). After developing, membranes were stained with India ink to show equal protein loading (bottom). Representative images from three experiments are shown. (D) WT and *hul5*Δ-null strains expressing Lys1-L146P, W353R, or V26D were subjected to CHX chase and Western blotting with α-GFP (top). Membranes were then stained with India ink (bottom). Representative images from three experiments are shown. (E–F) Formation of the ~37 kDa fragment is 26S-proteasome and PQC-E3-ligase dependent. (E) WT and *hul5*Δ*pdr5*Δ null cells expressing Lys1-V26D were grown into log phase, and *hul5*Δ*pdr5*Δ null cells were treated with either the proteasome inhibitor MG132 or the vehicle control DMSO. All samples were subjected to CHX chase and Western blotting with α-GFP (top). Membranes were then stained with India ink (bottom). Representative images from three experiments are shown. (F) WT, *hul5*Δ, and *hul5*Δ*san1*Δ*ubr1*Δ cells expressing Lys1-L146P were subjected to CHX chase and Western blotting with α-GFP (top). Membranes were then stained with India ink (bottom). Representative images from three experiments are shown. (G) Full-length Lys1-W353R proteolysis is faster in a *hul5*Δ null. WT and *hul5*Δ null cells expressing Lys1-W353R were subjected to CHX chase and Western blotting with α-GFP and α-Pgk1. The mean and SD of three experiments are shown.

stabilization of each substrate in a *hul5*Δ null background, a phenotype that was nonetheless rescued by *HUL5* complementation (Figure 5B; Supplemental Figure S14, B and C). The loss of Hul5 led to a complete stabilization of fluorescence but only a minor slowing of degradation of the full-length Lys1 substrates.

Hul5 is bound to the 26S proteasome and extends ubiquitin chains as an E4 ligase. It thereby promotes proteasomal processivity (Leggett *et al.*, 2002; Crosas *et al.*, 2006). The absence of Hul5, or its human ortholog UBE3C, causes diminished processivity and partial proteolysis of substrates, resulting in the release of polypeptide fragments from the proteasome (Kohlmann *et al.*, 2008; Aviram and Kornitzer, 2010; Chu *et al.*, 2013). When PQC substrates are fused to GFP or an enzyme, a stable fragment that encompasses functional GFP or enzyme can be created by partial proteolysis. Accordingly, a

*hul5*Δ null is often scored as a strong stabilizer in screens that utilize substrate-GFP or substrate-enzyme fusions: despite efficient delivery of ubiquitinated, full-length protein to the proteosome, optically or enzymatically active fragments are released and accumulate when Hul5 is absent.

We immunoblotted for such a fragment in CHX chases of Lys1-V26D, L29P, and I36D (Figure 5C; Supplemental Figure S14, D and E). In a *hul5*Δ null, each substrate produced a roughly 37 kDa fragment that was absent in the corresponding wild-type strain. The fragment markedly accumulated during chases, a trend that has also been observed when a *hul5*Δ null generates a functional Leu2 fragment (Kohlmann *et al.*, 2008), and upon complementation with *HUL5*, the fragment was no longer detectable.

We wondered if other Lys1-GFP variants would be proteolyzed to create a GFP fragment in a *hul5*Δ null. We therefore tested two Lys1 variants that are subject to San1-Ubr1-mediated degradation, the domain two mutant Lys1-L146P and the domain one mutant W353R. Like the San1-Ubr1-independent substrates already tested, Lys1-L146P and W353R were both partially proteolyzed in a *hul5*Δ null and an identical ~37kDa GFP fragment was detected (Figure 5D). Regardless of the E3 ligase that mediated their recognition, all Lys1-GFP substrates tested required Hul5 for complete proteolysis.

To confirm that the GFP fragment was a product of 26S proteasome activity, we treated *pdr5*Δ*hul5*Δ cells with MG132 and performed a CHX chase. Proteasome inhibition prevented the production of any additional ~37kDa fragment, strongly suggesting that it is a product of 26S proteasome activity (Figure 5E).

We also confirmed that Hul5 acted downstream of PQC E3 ligases. We again performed CHX chase of Lys1-L146P, a San1-Ubr1-dependent Lys1 substrate, and blotted for the ~37kDa fragment in a *san1*Δ*ubr1*Δ*hul5*Δ null background (Figure 5F). In the absence of E3 ligase activity, we were unable to detect any of the fragment, strongly suggesting that Hul5 acts downstream of recognition and ubiquitination.

While testing for fragment formation from Lys1-W353R and L146P, we observed what appeared to be *faster* initial processing of the full-length proteins in the *hul5*Δ null. We tested the rate of degradation of these substrates more directly in a CHX chase. In both cases (Figure 5G; Supplemental Figure S14F), we confirmed faster proteolysis of the full-length protein in the *hul5*Δ null background, a strong contrast to the slower proteolysis of full-length Lys1-V26D, L29P, and I36D (Supplemental Figure S14, B and C; Figure 5B). These data suggest that Hul5 does not universally increase proteolytic rate, and they provide a second example of distinct PQC outcomes caused by different mutants of Lys1, even those occurring within one domain.

Destabilizing substitutions at Lys1-W151 cause San1-Ubr1-mediated degradation, puncta formation, and proteotoxic stress

In the above screens, we occasionally identified two or three destabilizing substitutions at one residue position (ade1-L32P and L32R; ade1-G54E, G54R, and G54V; and lys1-W151G and W151R). These findings led us to consider a saturation mutagenesis approach in which a screen-identified position is substituted by all remaining amino acids. The resultant collection could be used to unveil the PQC pathways elicited by different "iso-positional" substitutions, and it promised to encompass a spectrum of misfolding, ranging from minimally to severely destabilized mutants. Iso-positional substrates would thereby allow us to investigate the relationship between misfoldedness (quantitated as degradation rate) and cytotoxicity.

To generate a rich panel of substrates, we sought a position that would be destabilized by most amino-acid substitutions. Lys1-W151 was a promising candidate, especially because both Lys1-W151G and W151R were well-defined San1-Ubr1 substrates (Figure 4B; Supplemental Figure S12A). It would be relatively straightforward to ascertain if other W151 variants were recognized and degraded by this comparatively simple PQC pathway.

To estimate the effect of the seventeen remaining W151 substitutions, we employed the FoldX energy function. FoldX uses solved crystal structures to calculate the thermodynamic effects of a substitution, and it has been employed to predict destabilizing variants in other studies (Guerois *et al.*, 2002; Schymkowitz *et al.*, 2005; Abildgaard *et al.*, 2019). To establish a benchmark, we first used FoldX to analyze all of our degraded Ade1 and Lys1 mutants. We found that each substrate had a ΔΔG of 4 kcal mol^{-1} or greater (Supplemental Table S4). We then used FoldX to analyze every possible substitution at W151. ΔΔGs ranged from 0.29 to 7.98 kcal mol^{-1} (Supplemental Table S5). Eleven of the remaining substitutions had ΔΔGs of 4 kcal mol^{-1} or greater, and only two substitutions (W151Y and W151F) had a ΔΔG of less than 1 kcal mol^{-1}, suggesting that saturation mutagenesis would yield many PQC substrates. We therefore chose W151 for further investigation.

To begin in vivo characterization, we performed a pilot screen that leveraged mixed-base oligonucleotide synthesis to introduce random codons at position 151 (Integrated DNA Technologies). Briefly, we ordered a primer in which the wild-type codon was replaced with three randomized bases, NNK. (N is any nucleotide; K is G or T. This mixed-base approach can yield codons for every amino acid but excludes two possible stop codons.) These primers were then used to make insert DNA for yeast recombination cloning, which assembled the randomly mutagenized codon and vector backbone into a full-length Lys1-W151X-GFP construct. YRC was performed in our *hrd2-1/HRD2* screening strain. Colonies bearing successful recombinants were predominantly dim and increased in fluorescence upon *HRD2* counterselection, again suggesting that few substitutions were tolerated and that most led to destabilization (unpublished data). We collected both substrates and stable mutants from this pilot screen, then used recombination cloning to create rarer codons that did not emerge from the screen, such as those for Met and Lys. All mutant-bearing plasmids were converted from *CEN/ARS* plasmids into stably integrating plasmids, as described above.

We transformed each member of the complete position-151 collection into a wild-type strain, and we performed CHX chases (Supplemental Figure S15). Lys1-W151Y and W151F were stable, as predicted by FoldX calculations (ΔΔGs 0.3 and 0.75 kcal mol^{-1}, respectively) and as might be expected of these conservative substitutions. However, FoldX calculations were not always sufficient for such predictions: Lys1-W151H was estimated to be strongly destabilizing (ΔΔG = 4 kcal mol^{-1}), but it was biologically stable (Supplemental Figure S15). Our iso-positional collection allowed us to uncover discrepancies between a well-established computational method and in vivo stability.

All other mutants were destabilized to varying degrees in a wild-type background (Figure 6, A–C; Supplemental Figure S15). In CHX chases, Lys1-W151P had the fastest degradation rate, reaching its half-life in roughly three hours. On the other hand, Lys1-W151L, W151M, and W151C were almost as stable as Lys1-GFP. We directly compared computational predictions with these in vivo measurements of degradation. For each mutant, FoldX ΔΔG was plotted against the percentage of fluorescence remaining after a three-hour-long CHX chase. A linear regression fit to those data had an R^2

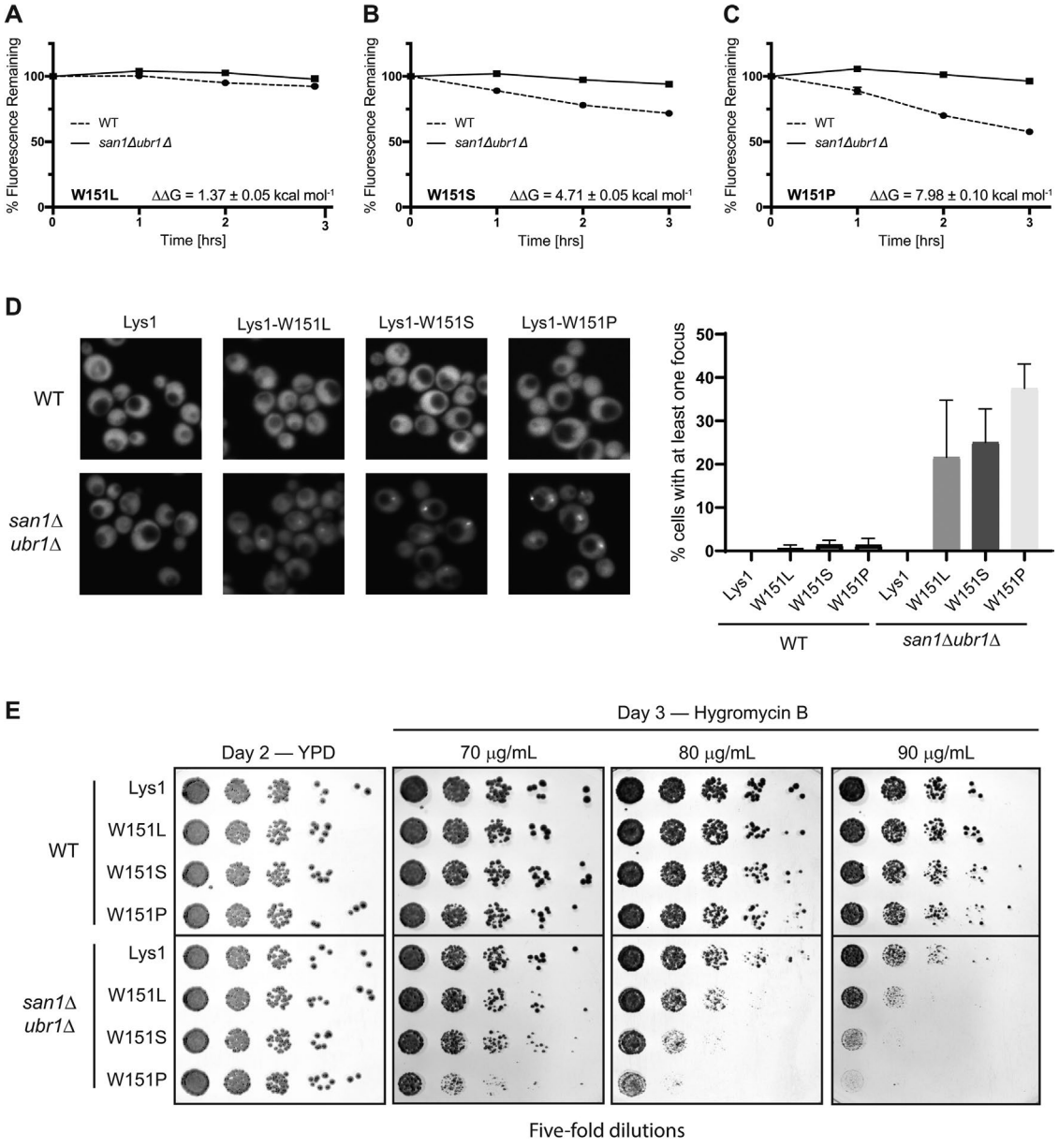

FIGURE 6: Destabilized Lys1-W151X variants form foci and cause toxicity in a *san1Δubr1Δ* null. (A–C) Three W151X mutants represent a range of degradation kinetics and computationally determined ΔΔGs. WT anzd *san1Δubr1Δ* null cells expressing Lys1-W151L (A), W151S (C), or W151P (D) were subjected to CHX chase. At the indicated timepoints, 10,000 cells were analyzed by flow cytometry. The mean and SD of three experiments are shown. These data are also shown in Supplemental Figure S15. FoldX-calculated ΔΔGs are shown for each mutant. The BuildModel function of FoldX was run three times for each mutant. Averages and SDs are shown. These data are also shown in Supplemental Table S4. (D) Destabilizing substitutions at Lys1-W151 form foci in vivo. WT and *san1Δubr1Δ* null strains expressing either Lys1-GFP or the indicated Lys1 mutant were grown into log phase. Cells were then imaged using confocal microscopy. Representative images are shown. At least 250 cells were visualized to quantitate the percentage of cells with at least one focus. The average and SD of three experiments are shown. (E) Destabilizing substitutions cause toxicity. WT and *san1Δubr1Δ* null strains expressing either Lys1-GFP or the indicated mutants were subjected to serial 1:5 dilutions followed by pinning onto YPD and hygromycin B plates (70, 80, 90 μg/ml). YPD plates were grown for two days at 30°C, and hygromycin B plates were grown for three days at 30°C. Representative images from three experiments are repeats are shown.

of 0.5 (Supplemental Figure S16), again suggesting that computational approaches are useful but imperfect.

To test if all destabilizing substitutions at position 151 were subject to San1-Ubr1-mediated degradation, we transformed each W151X mutant into a *san1Δubr1Δ* null background and performed CHX chase. As expected, the *san1Δubr1Δ* null background had no effect on Lys1-GFP or the stable mutants Lys1-W151Y, W151F, and W151H. In all other cases, the *san1Δubr1Δ* null background ablated degradation (Figure 6, A–C; Supplemental Figure S15). Even the very slowly degraded mutants Lys1-W151L, W151M, and W151C were stabilized in the absence of San1 and Ubr1, confirming that these variants were bona fide substrates. The same PQC pathway

recognized every destabilizing substitution, ranging from cavity formers to helix breakers.

We chose three mutants for further study: Lys1-W151L, W151S, and W151P, which have slow, intermediate, and fast degradation rates and ΔΔGs of 1.37, 4.71, and 7.96 kcal mol^{-1}, respectively (Figure 6, A–C). First, strains expressing these mutants were subjected to confocal microscopy in an effort to detect foci formation, a classical trait of misfolded proteins. In a wild-type background, Lys1-GFP, W151L, W151S, and W151P all produced a diffuse signal and no foci (Figure 6D, top). In a *san1*Δ*ubr1*Δ null background, Lys1-GFP again produced a diffuse signal, but Lys1-W151L, W151S, and W151P all produced foci in a significant proportion of cells (Figure 6D, bottom and graph). Even the least misfolded variant caused a cell-biological quality-control phenotype in the absence of PQC degradation.

Next, each variant was assayed for growth defects in wild-type and *san1*Δ*ubr1*Δ null backgrounds using a serial-dilution growth assay. Misfolded variants did not induce growth defects in either background on standard yeast extract-peptone-dextrose medium (Figure 6E, YPD). To further sensitize cells to proteotoxic stress, we performed growth assays on medium containing hygromycin B, which is thought to induce translational errors and is generally toxic to strains lacking PQC machinery (Brodersen *et al.*, 2000; Chuang and Madura, 2005; Bengtson and Joazeiro, 2010; Jaeger *et al.*, 2018; Niekamp *et al.*, 2019; Runnebohm *et al.*, 2020; Woodruff *et al.*, 2021). On hygromycin B plates, W151X variants caused no additional toxicity when expressed in a wild-type background (Figure 6E, top). By contrast, Lys1-W151P, W151S, and W151L caused toxicity in the *san1*Δ*ubr1*Δ background that corresponded with their degradation rates and ΔΔGs (Figure 6E, bottom). Cells expressing Lys1-W151P were inviable at 90 μg mL^{-1}; those expressing Lys1-W151S evinced a 25- to 125-fold decrease in viability at 80 and 90 μg mL^{-1}; and those expressing Lys1-W151L evinced a 5- to 25-fold decrease in viability at 80 and 90 μg mL^{-1}. Little or no additional outgrowth occurred when these strains were incubated on hygromycin B for six days at 30°C (unpublished data). San1 and Ubr1 ameliorated point-mutant toxicity across a range of misfoldedness. Notably, the ΔΔG of Lys1-W151L is roughly equivalent to the ΔΔG of the average translational error in *E. Coli* (Mordret *et al.*, 2019).

A variant of yeast chorismate mutase that undergoes ligand-mediated stabilization

Protein-ligand binding can facilitate folding and maturation in some instances (Van Goor *et al.*, 2009; Van Goor *et al.*, 2011; Pedemonte *et al.*, 2020), and it can induce misfolding and degradation in others (Shearer and Hampton, 2005; Garza *et al.*, 2009; Wangeline and Hampton, 2018; Gopal *et al.*, 2020). To create a simple model of either phenomenon, we set out to isolate minimally misfolded variants of an allosteric enzyme, aiming to repurpose the protein's allosteric effector as a pharmacological chaperone or a monovalent degrader. We reasoned that an ideal parent protein would be a soluble, homomeric, allosteric enzyme with a scorable function, known structure, and well-defined allosteric ligand and binding site. We therefore chose perhaps the simplest allosteric protein known, the enzyme chorismate mutase (Aro7 in yeast). This soluble, homodimeric enzyme occupies a branch point in the synthesis of tyrosine (Tyr) and tryptophan (Trp); it commits chorismate to Tyr synthesis and diverts it from Trp synthesis. To balance Trp and Tyr levels, CM activity is regulated by a simple allosteric mechanism: Trp activates it (favoring production of Tyr) while Tyr inhibits it (favoring production of Trp).

The structural basis of this Trp- and Tyr-mediated regulation is extraordinarily well-studied (Xue *et al.*, 1994; Sträter *et al.*, 1996). The CM homodimer has a ligand-binding site at the interface of the subunits, and structure-function analyses have identified mutations that block or disable allosteric binding (Schnappauf *et al.*, 1998). As importantly, *aro7*Δ nulls are tyrosine and phenylalanine auxotrophs, again allowing us to test mutant function with growth assays (Tang *et al.*, 1991), and a CM-GFP fusion was both stable and functional (Supplemental Figures S17 and S18). CM had the same useful characteristics of the above parent proteins.

We mutagenized *ARO7* with error-prone PCR, screened ~20,000 *aro7*-mutant-GFP colonies, and recovered three degraded point mutants at two positions: Aro7-R33G, D147G, and D147V. These functional-but-degraded mutants met our criteria for minimal misfolding (Supplemental Figure S18 and S19). In the Aro7 crystal structure (PDB 1CSM), both Aro7-R33 and D147 were buried in the protein, and hydrogen bonds were predicted between the carboxylic acid group of the D147 sidechain and the guanidino group of R33 (Supplemental Figure S20). For a third time, the screen yielded classically destabilizing substitutions, in this case at two residues that compose a structurally critical intramolecular interaction.

We tested these CM mutants for in vivo stabilization by Trp and Tyr. First, each mutant was grown in a range of Trp concentrations, and mutant steady-state levels were assayed by flow cytometry. While Aro7 and Aro7-D147V steady state-levels were relatively unchanged (Supplemental Figure S21A; Figure 7C), Aro7-R33G and D147G both showed dose-responsive stabilization (Figure 7, A and B). In both cases, saturation was achieved at roughly 1 mM Trp, and half-max stabilization was reached between 100 and 200 μM. As might be expected of an in vivo assay and a misfolded variant, this represented a four- to eight-fold decrease in apparent affinity compared with in vitro Aro7-Trp-binding assays, in which half-max binding was reached at roughly 25 μM Trp (Schmidheini *et al.*, 1990). In parallel experiments, each mutant was grown in a range of Tyr concentrations, but mutant steady-state levels neither increased nor decreased in response to the ligand (unpublished data).

Next, we directly tested the effect of Trp on degradation rates. Cells expressing Aro7, Aro7-R33G, D147G, and D147V were grown in medium lacking Trp or medium with 1 mM Trp, and CHX chase was performed by flow cytometry. Aro7-GFP (Supplemental Figure S21A) and Aro7-D147V (Figure 7C) chases were largely unaffected by the presence of Trp. On the other hand, both Aro7-D147G and R33G were markedly stabilized by the ligand (Figure 7, A and B). In two related assays, Aro7-R33G and D147G were pharmacologically chaperoned by Trp.

We were surprised that only one of the two substitutions at D147 could be stabilized by Trp (Figure 7, B and C), and we wondered if substitutions at R33 would also include both Trp-responsive and -nonresponsive mutants. In preliminary experiments, we found that Aro7-R33G stabilization by Trp could be visualized when cells were grown on solid media: Cells expressing *aro7-R33G* were significantly brighter on plates with 1 mM Trp than on plates lacking Trp (unpublished data). We leveraged this phenotype and saturation mutagenesis at R33 (achieved by the same method used to randomize the Lys1-W151 codon) to attempt to identify an R33 substitution that was Trp-nonresponsive. Dim mutant-bearing colonies were patched onto solid medium with or without 1 mM Trp, and patches that were dim on both media were preliminarily scored as Trp nonresponsive (unpublished data). From these efforts, we repeatedly recovered the mutant Aro7-R33P. Subsequent Trp dose responses and CHX chase confirmed that R33P could not be stabilized by Trp (Figure 7D).

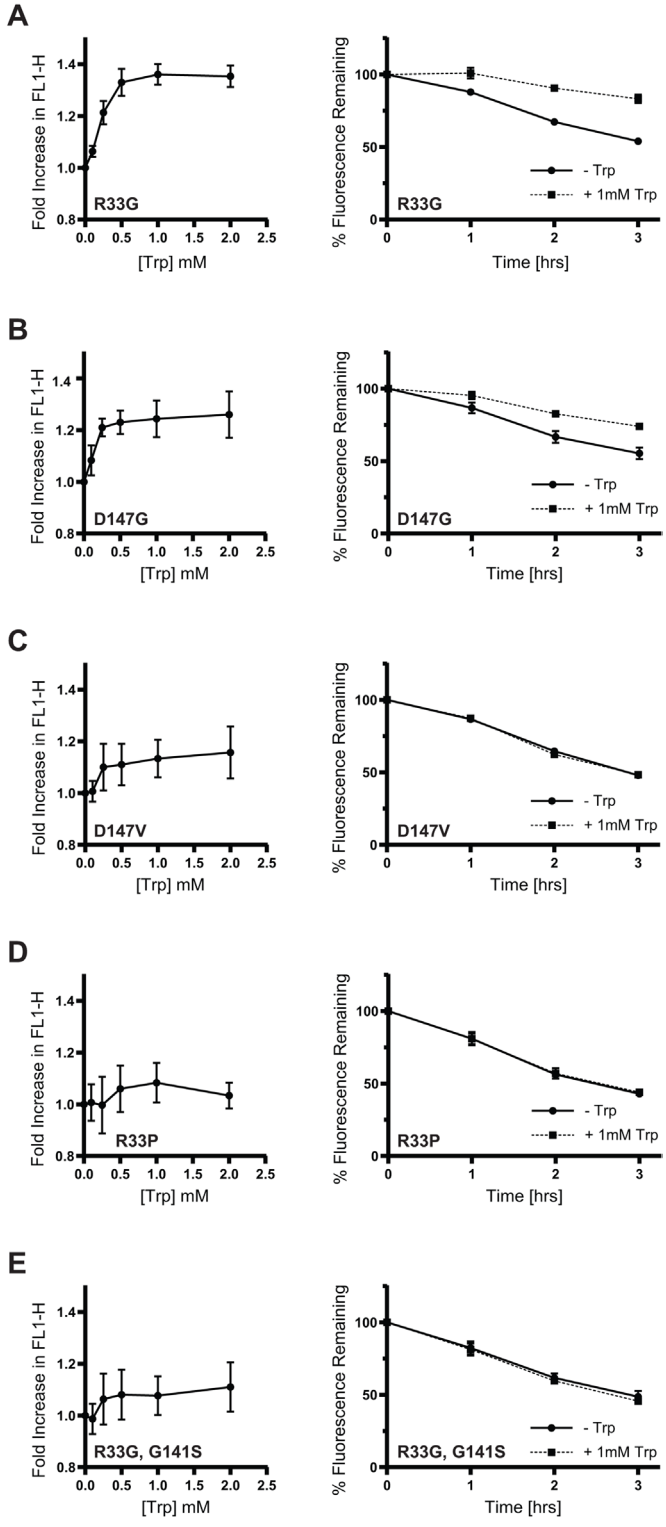

FIGURE 7: Binding-site specific stabilization of Aro7 mutants by Trp. (A–E, left) Trp dose responses. WT cells expressing the indicated Aro7 mutants were maintained in log phase overnight in media containing the indicated dosage of Trp. 10,000 cells from each dosage were then analyzed by flow cytometry. Data are normalized to the untreated, no Trp control. Mean and SD of three experiments are shown. (A–E, right) CHX chase with and without Trp. WT cells expressing the indicated Aro7 mutants were grown overnight in log phase in media containing either no Trp or 1 mM Trp. Cells were then treated with CHX, and 10,000 cells were analyzed by flow cytometry at the times indicated. The mean and SD of three experiments are shown.

A simple explanation for these observations would be that the more structurally destabilizing a substitution is, the more recalcitrant to stabilization by a pharmacological chaperone it will be. However, Trp responsiveness was not always predictable from computationally predicted ΔΔG (Supplemental Table S6). The Trp nonresponsive Aro7-D147V had a predicted ΔΔG of 2.7 kcal mol^{-1}, whereas the Trp-responsive Aro7-D147G had a predicted ΔΔG of 6.15 kcal mol^{-1}. Thus, responsiveness to a pharmacological chaperone can differ between substitutions at the same residue position in ways that defy explanation by in silico assessments of folding.

A final, defining feature of pharmacological chaperoning is that responsive substrates are stabilized by interactions between the drug and a bona-fide binding site (Tapper *et al.*, 2004; Generoso *et al.*, 2015). The allosteric Trp binding site of Aro7 can be blocked by the point mutation Aro7-G141S (Schnappauf *et al.*, 1998), and in control experiments, Aro7-G141S-GFP was stable and unaffected by Trp in steady-state-level and CHX chase assays (Supplemental Figure S21B). We therefore used the double mutant *aro7-R33G, G141S-GFP* to test whether the CM Trp binding was required for mutant stabilization. In strong contrast to Aro7-R33G (Figure 7A), Aro7-R33G, G141S-GFP could not be stabilized by Trp in either steady-state or CHX-chase experiments (Figure 7E). Both effects required the native Aro7 allosteric site.

DISCUSSION

A wide variety of polypeptide species can be described as misfolded, ranging from those that lack a stable shape—such as random amino-acid sequences—to those that retain structure-dependent functions—such as enzyme activity (Biederer *et al.*, 1996; Rosenbaum *et al.*, 2011). PQC degrades substrates spanning this entire spectrum, suggesting that disparate misfolded species can be recognized by their common biochemical features. Identifying those features has been a longstanding goal of biological and biomedical research, and some facets of PQC recognition have been revealed by screens that generate and characterize PQC substrates (Gilon *et al.*, 2000; Geffen *et al.*, 2016; Maurer *et al.*, 2016). Yet, this systematic approach has not been applied to misfolded proteins that closely resemble native structures. We therefore developed a screen to systematically generate and study instances of minimal misfolding. The screen is an orthogonal complement to studies that have used degron libraries, systematic truncations, and misfolded hypomorphic mutants derived from classical genetics (Biederer *et al.*, 1996; Plemper *et al.*, 1998; Gardner *et al.*, 2005; Ravid *et al.*, 2006; Nakatsukasa *et al.*, 2008; Farzin *et al.*, 2012), and it creates models of both disease-causing mutants and the translational errors that occur continuously in all cells (Klaips *et al.*, 2018; Matreyek *et al.*, 2018).

Because we screened simple, monomeric parent proteins, we were able to use solved native structures as both mnemonic and predictive tools. Every mutant we isolated, purely by phenotype, caused a classical structural destabilization, such as charge imposition, steric clash, and cavity formation (Yue *et al.*, 2005; Redler *et al.*, 2016). These intuitive results allowed us to leverage the Lys1 structure and two screen-isolated mutants, Lys1-V26D and L29P, to design Lys1-I36D. Upon testing, Lys1-I36D was not only subject to PQC degradation but was also recognized by the same atypical quality-control pathway as Lys1-V26D and L29P. Screen-isolated substrates and solved crystal structures allowed us to connect destabilizing substitutions and PQC outcomes.

Our substrate collections thereby allowed us to discern some testable "rules" of minimal misfolding, as well as some surprises and caveats. At an individual amino-acid position, all destabilizing

substitutions were recognized by the same quality-control pathway: Sixteen different destabilizing substitutions at Lys1-W151 caused degradation by San1 and Ubr1 in parallel. However, it was unclear which substitutions would destabilize the protein. Lys1-W151H was predicted to be highly destabilizing by the FoldX energy function, but the mutant was a stable protein in vivo. FoldX ΔΔGs were also insufficient to predict which Aro7-R33 and D147 mutants could be pharmacologically chaperoned. Aro7-R33G (6.38 kcal mol^{-1}) and D147G (6.15 kcal mol^{-1}) were stabilized by Trp, but R33P (8.51 kcal mol^{-1}) and D147V (2.6 kcal mol^{-1}) were not. Iso-positional mutants unveiled a spectrum of degradation rates, cytotoxicity, and responsiveness to a pharmacological chaperone, as might have been expected, but those properties often defied in silico prediction and required in vivo characterization.

Destabilizing substitutions at different residue positions could cause surprisingly varied PQC responses, but Ade1 and Lys1 mutants nevertheless unveiled discernable trends and testable hypotheses. In the case of Ade1, every screen-isolated mutant seemed to cause a similar, if complex, PQC response. In the case of Lys1, even mutants within one domain were recognized by distinct PQC pathways. Yet, as a rule, Lys1 mutants that were closely grouped in the tertiary structure caused similar PQC responses, and this spatial rubric could be extended to processing by the 26S proteasome and the E4 ligase Hul5. Hul5 was required for complete proteolysis of all Lys1 mutants tested, but the effect of Hul5 on the proteolysis of full-length mutants differed. In a *hul5*Δ null background, grouped San1-Ubr1-independent mutants were processed slower, whereas spatially distinct, San1-Ubr1 mutants were processed faster. In vivo characterization was essential to these studies as well, and computational prediction offered limited insight. While FoldX predicted that our Ade1 and Lys1 mutants would be destabilized, it often failed to predict relative degradation rates, a shortcoming noted elsewhere (Nielsen *et al.*, 2017). Ade-L32R (5.3 kcal mol^{-1}) had a half-life of roughly 30 min, whereas Ade1-L102P (8.4 kcal mol^{-1}) had a half-life of roughly 5.8 h. Lys1-V26D (4.26 kcal mol^{-1}) had a half-life of roughly 45 min, whereas Lys1-P194Q (5.34 kcal mol^{-1}) had a half-life of roughly 11.3 h.

Altogether, we believe these observations support a model of minimal misfolding as a "local" rather than "global" perturbation of protein structure. In cases of "local" misfolding, a structural disturbance is confined to a small area of the protein while the remainder of the structure and function remain relatively unaffected (Stein *et al.*, 2019). By contrast, "global" misfolding destabilizes the entire polypeptide and function is lost. A number of in silico studies suggest that PQC substrates could possess minimal, local changes to structure. When it was modeled computationally, a misfolded variant of the PDZ domain had rearranged secondary structures that caused only minor changes to solvent-exposed surface area (Gianni *et al.*, 2010). Similarly, computational analyses of aspartoacylase and a PQC-degraded variant, aspartoacylase C152W, showed no substantial differences between the wild-type and mutant structures, highlighting the subtlety of the structural change and re-emphasizing the limitations of computational approaches (Gersing *et al.*, 2021).

In our work and others', a model of "local" misfolding is also supported by in vivo characterization of different misfolded variants of a single protein. Destabilized MSH2 mutants that are grouped in one region of the protein's tertiary structure are temperature-sensitive for degradation, whereas other mutants in other regions of the protein are temperature-insensitive, suggesting at least two distinct modes of misfolding (Nielsen *et al.*, 2017). Alongside our analysis of Lys1, these findings imply that the destabilized variants of a functionally complex, multimeric human protein could include diverse, potentially cytotoxic species, underlining the challenge that minimally misfolded proteins pose for PQC.

If local misfolding unveils a "degron," as has been suggested by many investigators (Fredrickson *et al.*, 2011; Furth *et al.*, 2011; Gersing *et al.*, 2021), it remains unclear how a structural perturbation and a quality-control degron are spatially related. Degrons are often thought to be linear amino-acid sequences in near proximity to a destabilizing mutation, but it is unclear how that rule would apply to spatially distant Ade1 substitutions, all of which seem to present a San1-Doa10 degradation signal. Perhaps a destabilizing substitution can cause local misfolding at a distant site in a protein, just as allosteric effectors and amino-acid substitutions can influence the properties of a distant active site (Brinkmann-Chen *et al.*, 2013; Guo and Zhou, 2016). Perhaps the degradation signal unveiled by minimal misfolding can be distributed across a structure rather than confined to a linear sequence (Gardner and Hampton, 1999). Hydrogen-deuterium exchange and mass spectrometry of our mutants would allow us to test these hypotheses.

Based on previous studies, minimal misfolding of soluble proteins might be expected to present hydrophobicity to solution (Fredrickson *et al.*, 2011; Rosenbaum *et al.*, 2011; Fredrickson *et al.*, 2013). Indeed, degradation can be triggered by a bivalent small molecule that binds to a target protein and thereby appends a hydrophobic group to the protein's surface (Neklesa *et al.*, 2011). We were somewhat surprised, then, that our screen did not identify a single instance in which a solvent-exposed hydrophilic residue was substituted by a hydrophobic amino acid. It is possible that a single substitution is insufficient to cause degradation, but it also seems increasingly likely that the biochemical PQC "code" is quite complex. The most recent high-throughput degron screen did not identify consensus biochemical features amongst amino-acid sequences that caused degradation (Geffen *et al.*, 2016), and the authors suggest that different PQC ligases may respond to distinct biochemical signals. Well-characterized, minimally misfolded substrates offer an opportunity to test that hypothesis and to characterize ligase-specific signals that are exposed upon misfolding.

In the cell, misfolded proteins are also recognized by molecular chaperones, and those chaperones are often required for ligases to recognize and ubiquitinate their substrates (Murata *et al.*, 2001; Nishikawa *et al.*, 2001; McClellan *et al.*, 2005; Kriegenburg *et al.*, 2014; Singh *et al.*, 2020). In those instances, the role of some chaperones rises above canonical disaggregase or holdase functions: Even when a Ubr1 substrate is immobilized in vitro on a silica bead and thereby prevented from aggregating, binding of Ubr1 to the substrate remains strongly dependent on the molecular chaperone Hsp70, and ubiquitination requires both Hsp70-ATPase and J-protein-cochaperone activity (Singh *et al.*, 2020). Our substrates present opportunities to further characterize the chaperones that participate in degradative PQC, and to investigate how those chaperones contribute to recognition and ubiquitination.

Altogether, the subtleties of misfolding and PQC degradation present considerable obstacles for drugs that aim to stabilize mutant proteins. Fortunately, pharmacological chaperoning appears to be a very generalizable approach: Using chorismate mutase as a parent protein, we were able to create a simple model of the phenomena (Pike *et al.*, 2001; Van Goor *et al.*, 2011; Cornella-Taracido and Garcia-Echeverria, 2020; Pedemonte *et al.*, 2020). However, even in the case of CM mutants, pharmacological chaperoning was not universally effective. It is also worth noting that ΔF508-CFTR correctors are not a standalone treatment, but rather are administered

in conjunction with "potentiators" that improve mutant-protein function (Van Goor *et al.*, 2009; Rowe and Verkman, 2013). Nevertheless, pharmacological chaperones and monovalent degraders remain powerful therapeutic tools, and we are continuing to screen for "mallosteric" CM mutants.

The complexities revealed by our screens and follow-up studies suggest a different line of inquiry from the venerated "protein folding problem": the protein *mis*folding problem. It is likely that PQC encounters an array of differently misfolded and damaged versions of each protein in the proteome, and these variants can impose significant proteotoxicity. In mice, mutations that lower translation fidelity cause neurodegeneration (Lee *et al.*, 2006; Vo *et al.*, 2018). The mutations that destabilize protein structure, the polypeptide species that arise upon misfolding, and the proteotoxicity that those species can cause remain exigent topics in the field. Minimal misfolding is central to those concerns, and our screen offers tractable models of the nuanced PQC phenomena that shroud a growing list of debilitating proteinopathies.

MATERIALS AND METHODS

Request a protocol through *Bio-protocol*.

Yeast and bacteria growth media

Yeast strains were grown at 30°C with aeration in minimal medium (Difco yeast nitrogen base with necessary amino acids and nucleic acids) with 2% glucose or rich medium (YPD). *E. coli* DH5α were grown at 37°C in LB medium with ampicillin.

Plasmids and strains

Supplemental Table S7 lists the plasmids used in these studies. Some were made using standard techniques as previously described (Sato *et al.*, 2009), but the majority were constructed using yeast recombination cloning (Muhlrad *et al.*, 1992). In the case of mutants isolated during screens, we used yeast recombination cloning and an integrating-after-CEN-excision approach described elsewhere (Flagg *et al.*, 2019). Primer sequences are not shown but can be provided upon request (Supplemental Table S9). All plasmids made during these studies were sequenced verified (Eton Biosciences) and are being prepared for deposit at AddGene.

Supplemental Table S8 lists the yeast strains used in these studies. The screen strains were derived from S288C (RHY2863). All other strains were derived from BY4741. We used the standard LiOAc method (Ito *et al.*, 1983) for yeast transformations. A number of null strains were obtained from the yeast deletion collection (Winzeler *et al.*, 1999). The null strains used in Supplemental Figure S13 are from the TUS 2.1 collection (Hickey *et al.*, 2021). Otherwise, knockouts were made using a PCR-mediated approach involving a selectable marker (NatMX, KanMX, or HphMX) flanked by 50bp directly upstream and downstream of the gene to be deleted. When this method was used, transformants were grown out on YPD plates, then lawns were replica plated onto drug-selection plates (CloNat/nourseothricin, G418, or hygromycin). All deletions were confirmed using PCR.

Random mutagenesis

Mutazyme II (Agilent) was used to perform random mutagenesis according to the manufacturer's instructions for low rates of mutagenesis, including a reduced number of PCR cycles and high concentration of template DNA. Mutagenic PCR yield was quantitated by gel electrophoresis, imaging, and band quantitation (Protein Simple). Sample with mutated DNA was then treated with DpnI (NEB) to remove template DNA, and this sample was then used as an amplicon for an additional, nonmutagenic PCR using high-fidelity Phusion polymerase (NEB). The product of this PCR was then used as the insert in yeast recombination cloning for the screen, and new product was generated from the original mutated stock, as needed.

Structure-misfunction screening

A relevant screen strain was transformed with BamHI-XhoI digested pRH2940 and the appropriate mutated amplicon at a 1:9 ratio. Transformants were grown on -Leu -Ura plates that selected for the recombined plasmid and the *HRD2-URA3 CEN* plasmid. Transformants were grown for 3 d before observation beneath a GFP-visualizing set up described elsewhere (Cronin and Hampton, 1999). Dim colonies were picked and patched to -Leu -Ade, -Leu -Lys, or -Leu -Tyr plates for Ade1, Lys1, and Aro7 mutants, respectively. Transformant plates were then allowed to grow overnight at room temperature before rescreening for and picking of additional dim colonies. Putatively functional mutants supported outgrowth of patches on drop out plates.

Grown patches were then streaked to both -Leu -Ura and -Lue 5-FOA plates for overnight growth. Throughout the following day, corresponding patches were monitored for increased fluorescence on the -Leu 5-FOA plates. Patches bearing putative substrates were then repatched from -Leu -Ura and -Leu 5FOA to -Lue plates. The next day, direct side-by-side comparisons were made, and patches that were brighter after counterselection were isolated for flow cytometry, plasmid isolation, and *CEN* excision, as described elsewhere (Flagg *et al.*, 2019).

Flow cytometry

GFP fluorescence was measured using a BD Accuri C6 flow cytometer (BD Biosciences) as previously described (Garza *et al.*, 2009). Ten thousand cells are analyzed in all readings. Statistics were recorded from BD Accuri software.

In vivo stabilization by glycerol

Relevant yeast strains were grown into log phase, pelleted at 5000 rpm in a microcentrifuge for 5 min, then resuspended in YNB -Leu +20% glycerol medium. Time zero readings were then taken on a flow cytometer. Cells were then incubated for 6 h at 30°C with aeration, after which final readings were taken on a flow cytometer. All readings represent 10,000 cells.

Whole cell lysates and western blotting

At each timepoint, three OD eq of cells were harvested and centrifuged at 14,000 × g for 2 min. Cell pellets were then resuspended in 100 µl SUME buffer (1% SDS, 8 M urea, 10 mM MOPS, 10 mM EDTA, pH 6.8) with protease inhibitors (1 mM phenylmethylsulfonyl fluoride, 260 mM 4-(2-aminoethyl) benzenesulfonyl fluoride hydrochloride, 100 mM leupeptin hemisulfate, 76 mM pepstatin A, 5 mM 6-aminocaproic acid, 5 mM benzamidine, and 142 mM TPCK). Silica beads were then added, and cells were lysed on a multivortexer (1 min of vortexing at room temperature followed by 1 min on ice, repeated three times). A 100 µl of 2X urea sample buffer (8 M urea, 4% SDS, 200 mM dithiothreitol, 125 mM Tris, pH 6.8) was added to each lysed sample, and the mixture was then boiled at 95°C for 8 min. Finally, samples were centrifuged at 14,000 × g for 5 min.

In all cases, samples were resolved on 10% acrylamide gels by SDS–PAGE, transferred to nitrocellulose in 13% methanol, and blotted with mouse monoclonal anti-GFP antibody (Living Colors) or anti-PGK1 antibody (Molecular Probes) followed by goat anti-mouse HRP-conjugated secondary antibody (Jackson ImmunoResearch).

Cycloheximide chase

CHX chases were performed as described elsewhere (Sato *et al.*, 2009). Yeast strains were grown in minimal medium to early log phase (OD_{600} < 0.6) before the addition of cycloheximide at a final concentration of 50 µg/ml. Samples were taken at the indicated time points and subjected to lysis, resolution by SDS–PAGE, and immunoblotting. Alternatively, cells were subjected to flow cytometry at the indicated timepoints, as described above.

MG132 treatment

In all MG132 experiments, MG132 was added to 25 µg/ml, or an equal volume of DMSO vehicle control was used. In the majority of cases, this was followed by a 2-h incubation period to allow for full proteasomal inhibition. However, in the case of Figure 5E, we added MG132 and immediately proceeded with the experiment shown.

In vivo stabilization by Trp

Cells were grown overnight in minimal medium lacking Trp. Stationary-phase overnight cultures were then grown into log phase in minimal medium lacking Trp. These log-phase cells were then diluted to 0.0001 OD ml^{-1} in minimal media with final concentrations of 0 mM, 0.01 mM, 0.1 mM. 0.25 mM, 0.5 mM, 1 mM, or 2 mM Trp. Dose–response cultures were then incubated with aeration overnight at 30°C, and the following day, log-phase overnight cultures were subjected to flow cytometry to determine steady-state fluorescence.

To perform chases, CHX was added to the 1 mM Trp log-phase overnight cultures and the no-Trp log-phase overnight cultures. Flow cytometry was then performed at the timepoints indicated.

Computational ΔΔG calculations

In all cases, FoldX was used as a plugin to the YASARA graphical user interface (Land and Humble, 2018). The RepairPDB FoldX function was applied to Ade1 (PDB 1A48), Lys1 (PDB 2QRL), and Aro7 (PDB 1CSM). The BuildModel function was then used to calculate the ΔΔG of each substitution generated by the screen. In each case, the function was run three times. Averages and SDs are reported.

Microscopy and foci quantitation

Images were taken on a Zeiss Axiovert 200M fluorescent microscope with a CSU-X1 spinning disk (Yokogawa), a Chrome MLE laser source (Toptica Photonics), and µManager v1.4 software. In each image, a 2-µm Z-stack with 0.25-µm slices was acquired using a Nikon 40× 0.65-NA oil objective. For each strain, at least 200 cells were imaged from nonoverlapping fields of view. Optimal Z-projections were compiled in FIJI. Images were then blinded and scored manually. At least 200 cells were scored in each case.

Visualization and representation of protein structure

All molecular graphics and analyses performed with UCSF Chimera, developed by the Resource for Biocomputing, Visualization, and Informatics at the University of California, San Francisco, with support from National Institute of Health P41-GM103311.

ACKNOWLEDGMENTS

These studies were supported by National Institutes of Health Grant 5R01DK051996-27 (to R.Y.H.). M.P.F. was also supported by National Institutes of Health Cell Molecular Genetics (CMG) Training Grant 5T32GM007240-37. The authors thank Mark Hochstrasser and his lab for providing the TUS 2.1 collection. The authors would also like to thank members of the Hampton lab, past and present, for their creativity, thoughtful criticism, friendship, and countless handfuls of trail mix. Days in lab often felt like days at summer camp. R.Y.H. would like to acknowledge the support of his recently departed, preternaturally wonderful, and locally famous black cat Carbon who passed unexpectedly to the chagrin of all. We dedicate this paper to the memory of Alfred Goldberg (Harvard), who passed in April of 2023. He was a founding giant of proteolysis, a career-long friend to R.Y.H., a fantastic mentor to many, a joyous and funny colleague, a prolific and broadly impactful scientist, and a creative impromptu poet. You will be deeply missed; thank you for all you did and gave.

REFERENCES

Abildgaard AB, Stein A, Nielsen SV, Schultz-Knudsen K, Papaleo E, Shrikhande A, Hoffmann ER, Bernstein I, Gerdes AM, Takahashi M, *et al.* (2019). Computational and cellular studies reveal structural destabilization and degradation of mlh1 variants in lynch syndrome. ELife 8, e49138.

Al-Saryi NA, Al-Hejjaj MY, van Roermund CWT, Hulmes GE, Ekal L, Payton C, Wanders RJA, Hettema EH (2017). Two NAD-linked redox shuttles maintain the peroxisomal redox balance in Saccharomyces cerevisiae. Sci Rep 7, 11868.

Aviram S, Kornitzer D (2010). The ubiquitin ligase Hul5 promotes proteasomal processivity. Mol Cell Biol 30, 985–994.

Auton M, Bolen DW (2015). Predicting the energetics of osmolyte-induced protein folding/unfolding. Proc Natl Acad Sci USA 102, 15065–15068.

Bengtson MH, Joazeiro CAP (2010). Role of a ribosome-associated E3 ubiquitin ligase in protein quality control. Nature 467, 470–473.

Bernier V, Bichet DG, Bouvier M (2004a). Pharmacological chaperone action on G-protein-coupled receptors. Curr Opin Pharmacol 4, 528–533.

Bernier V, Lagacé M, Lonergan M, Arthus MF, Bichet DG, Bouvier M (2004b). Functional rescue of the constitutively internalized V2 vasopressin receptor mutant R137H by the pharmacological chaperone action of SR49059. Mol Endocrinol 18, 2074–2084.

Biederer T, Volkwein C, Sommer T (1996). Degradation of subunits of the Sec61p complex, an integral component of the ER membrane, by the ubiquitin-proteasome pathway. EMBO J 15, 2069–2076.

Breckel CA, Hochstrasser M (2021). Ubiquitin ligase redundancy and nuclear-cytoplasmic localization in yeast protein quality control. Biomolecules 11, 1821.

Brinkmann-Chen S, Flock T, Cahn JK, Snow CD, Brustad EM, McIntosh JA, Meinhold P, Zhang L, Arnold FH (2013). General approach to reversing ketol-acid reductoisomerase cofactor dependence from NADPH to NADH. Proc Natl Acad Sci USA 110, 10946–10951.

Brodersen DE, Clemons WM, Carter AP, Morgan-Warren RJ, Wimberly BT, Ramakrishnan V (2000). The structural basis for the action of the antibiotics tetracycline, pactamycin, and hygromycin B, on the 30S ribosomal subunit. Cell 103, 1143–1154.

Burk DL, Hwang J, Kwok E, Marrone L, Goodfellow V, Dmitrienko GI, Berghuis AM (2007). Structural studies of the final enzyme in the α-aminoadipate pathway-saccharopine dehydrogenase from Saccharomyces cerevisiae. J Mol Biol 373, 745–754.

Cagiada M, Johansson KE, Valanciute A, Nielsen SV, Hartmann-Petersen R, Yang JJ, Fowler DM, Stein A, Lindorff-Larsen K (2021). Understanding the origins of loss of protein function by analyzing the effects of thousands of variants on activity and abundance. Mol Biol Evol 38, 3235–3246.

Chu BW, Kovary KM, Guillaume J, Chen LC, Teruel MN, Wandless TJ (2013). The E3 ubiquitin ligase UBE3C enhances proteasome processivity by ubiquitinating partially proteolyzed substrates. J Biol Chem 288, 34575–34587.

Chua NK, Howe V, Jatana N, Thukral L, Brown AJ (2017). A conserved degron containing an amphipathic helix regulates the cholesterol-mediated turnover of human squalene monooxygenase, a rate-limiting enzyme in cholesterol synthesis. J Biol Chem 292, 19959–19973.

Chuang SM, Madura K (2005). Saccharomyces cerevisiae Ub-conjugating enzyme Ubc4 binds the proteasome in the presence of translationally damaged proteins. Genetics 171, 1477–1484.

Cornella-Taracido I, Garcia-Echeverria C (2020). Monovalent protein-degraders – Insights and future perspectives. Bioorg Med Chem Lett 30, 127202.

Cronin SR, Hampton RY (1999). Measuring protein degradation with green fluorescent protein. Methods Enzymol 302, 58–73.

Crosas B, Hanna J, Kirkpatrick DS, Zhang DP, Tone Y, Hathaway NA, Buecker C, Leggett DS, Schmidt M, King RW, *et al.* (2006). Ubiquitin

chains are remodeled at the proteasome by opposing ubiquitin ligase and deubiquitinating activities. Cell 127, 1401–1413.
Dikic I (2017). Proteasomal and autophagic degradation systems. Annu Rev Biochem 86, 193–224.
Eisele F, Wolf DH (2008). Degradation of misfolded protein in the cytoplasm is mediated by the ubiquitin ligase Ubr1. FEBS Lett 582, 4143–4146.
Fang NN, Ng AHM, Measday V, Mayor T (2011). Hul5 HECT ubiquitin ligase plays a major role in the ubiquitylation and turnover of cytosolic misfolded proteins. Nat Cell Biol 13, 1344–1352.
Farzin K-K, Fang NN, Ng AHM, Winget JM, Comyn SA, Mayor T (2012). The yeast ubr1 ubiquitin ligase participates in a prominent pathway that targets cytosolic thermosensitive mutants for degradation. G3 2, 619–628.
Flagg MP, Kao A, Hampton RY (2019). Integrating after CEN excision (ICE) plasmids: Combining the ease of yeast recombination cloning with the stability of genomic integration. Yeast 36, 593–605.
Foresti O, Rodriguez-Vaello V, Funaya C, Carvalho P (2014). Quality control of inner nuclear membrane proteins by the Asi complex. Science 346, 751–755.
Foresti O, Ruggiano A, Hannibal-Bach HK, Ejsing CS, Carvalho P (2013). Sterol homeostasis requires regulated degradation of squalene monooxygenase by the ubiquitin ligase Doa10/Teb4. ELife 2013, 1–17.
Fredrickson EK, Rosenbaum JC, Locke MN, Milac TI, Gardner RG (2011). Exposed hydrophobicity is a key determinant of nuclear quality control degradation. Mol Biol Cell 22, 2384–2395.
Fredrickson EK, Gallagher PS, Candadai SVC, Gardner RG (2013). Substrate recognition in nuclear protein quality control degradation is governed by exposed hydrophobicity that correlates with aggregation and insolubility. J Biol Chem 288, 6130–6139.
Furth N, Gertman O, Shiber A, Alfassy OS, Cohen I, Rosenberg MM, Doron NK, Friedler A, Ravid T (2011). Exposure of bipartite hydrophobic signal triggers nuclear quality control of Ndc10 at the endoplasmic reticulum/nuclear envelope. Mol Biol Cell 22, 4726–4739.
Gardner RG, Hampton RY (1999). A "distributed degron" allows regulated entry into the ER degradation pathway. EMBO J 18, 5994–6004.
Gardner RG, Nelson ZW, Gottschling DE (2005). Degradation-mediated protein quality control in the nucleus. Cell 120, 803–815.
Garofalo R, Wohlgemuth I, Pearson M, Lenz C, Urlaub H, Rodnina MV (2019). Broad range of missense error frequencies in cellular proteins. Nucleic Acids Res 47, 2932–2945.
Garza RM, Tran PN, Hampton RY (2009). Geranylgeranyl pyrophosphate is a potent regulator of HRD-dependent 3-hydroxy-3-methylglutaryl-CoA reductase degradation in yeast. J Biol Chem 284, 35368–35380.
Geffen Y, Appleboim A, Gardner RG, Friedman N, Sadeh R, Ravid T (2016). Mapping the landscape of a eukaryotic degronome. Mol Cell 63, 1055–1065.
Generoso SF, Giustiniano M, La Regina G, Bottone S, Passacantilli S, Di Maro S, Cassese H, Bruno A, Mallardo M, Dentice M, *et al.* (2015). Pharmacological folding chaperones act as allosteric ligands of Frizzled4. Nat Chem Biol 11, 280–286.
Gersing SK, Wang Y, Grønbæk-Thygesen M, Kampmeyer C, Clausen L, Willemoës M, Andréasson C, Stein A, Lindorff-Larsen K, Hartmann-Petersen R (2021). Mapping the degradation pathway of a disease-linked aspartoacylase variant. PLoS Genet 17, 1–28.
Gianni S, Ivarsson Y, De Simone A, Travaglini-Allocatelli C, Brunori M, Vendruscolo M (2010). Structural characterization of a misfolded intermediate populated during the folding process of a PDZ domain. Nat Struct Mol Biol 17, 1431–1437.
Gilon T, Chomsky O, Kulka RG (2000). Degradation signals recognized by the Ubc6p-Ubc7p ubiquitin-conjugating enzyme pair. Mol Cell Biol 20, 7214–7219.
Gopal P, Sarathy JP, Yee M, Ragunathan P, Shin J, Bhushan S, Zhu J, Akopian T, Kandror O, Lim TK, *et al.* (2020). Pyrazinamide triggers degradation of its target aspartate decarboxylase. Nat Commun 11, 1–10.
Guerois R, Nielsen JE, Serrano L (2002). Predicting changes in the stability of proteins and protein complexes: A study of more than 1000 mutations. J of Mol Biol 320, 369–387.
Guerriero CJ, Brodsky JL (2012). The delicate balance between secreted protein folding and endoplasmic reticulum-associated degradation in human physiology. Physiol Rev 92, 537–576.
Guo J, Zhou HX (2016). Protein allostery and conformational dynamics. Chem Rev 116, 6503–6515.
Harrington DJ, Adachi K, Royer WE (1997). The high resolution crystal structure of deoxyhemoglobin S. J Mol Biol 272, 398–407.
Hampton RY, Gardner RG, Rine J (1996). Role of 26S proteasome and HRD genes in the degradation of 3-hydroxy-3-methylglutaryl-CoA reductase, an integral endoplasmic reticulum membrane protein. Mol Biol Cell 7, 2029–2044.
Hawthorne DC, Mortimer RK (1960). Chromosome mapping in Saccharomyces: Centromere-linked genes. Genetics 45, 1085–1085110.
Heck JW, Cheung SK, Hampton RY (2010). Cytoplasmic protein quality control degradation mediated by parallel actions of the E3 ubiquitin ligases Ubr1 and San1. Proc Natl Acad Sci USA 107, 1106–1111.
Hickey CM, Breckel C, Zhang M, Theune WC, Hochstrasser M (2021). Protein quality control degron-containing substrates are differentially targeted in the cytoplasm and nucleus by ubiquitin ligases. Genetics 217, 1–19.
Howe V, Chua NK, Stevenson J, Brown AJ (2015). The regulatory domain of squalene monooxygenase contains a re-entrant loop and senses cholesterol via a conformational change. J Biol Chem 290, 27533–27544.
Huh WK, Falvo JV, Gerke LC, Carroll AS, Howson RW, Weissman JS, O'Shea EK (2003). Global analysis of protein localization in budding yeast. Nature 425, 686–691.
Ingram BVM (1957). Gene mutations in human haemoglobin: Difference between normal and sickle cell haemoglobin. Nature 180, 326–328.
Ito H, Fukuda Y, Murata K, Kimura A (1983). Transformation of intact yeast cells treated with alkali cations. J Bacteriol 153, 163–168.
Jaeger PA, Ornelas L, McElfresh C, Wong LR, Hampton RY, Ideker T (2018). Systematic gene-to-phenotype arrays: A high-throughput technique for molecular phenotyping. Mol Cell 69, 321–333.e3.
Jayaraj GG, Hipp MS, Ulrich Hartl F (2020). Functional modules of the proteostasis network. Cold Spring Harb Perspect Biol 12, a033951.
Jia X, Burugula BB, Chen V, Lemons RM, Jayakody S, Maksutova M, Kitzman JO (2021). Massively parallel functional testing of MSH2 missense variants conferring Lynch syndrome risk. Am J Hum Genet 108, 163–175.
Johnson PR, Swanson R, Rakhilina L, Hochstrasser M (1998). Degradation signal masking by heterodimerization of MATα2 and MATa1 blocks their mutual destruction by the ubiquitin-proteasome pathway. Cell 94, 217–227.
Jones EE, Broquist HP (1965) Saccharopine, An Intermediate of The Aminoadipic Acid Pathway of Lysine Biosynthesis. II. Studies in Saccharomyces Cereviseae. J Biol Chem 240, 2531–2536.
Juszkiewicz S, Hegde RS (2018). Quality control of orphaned proteins. Mol Cell 71, 443–457.
Khmelinskii A, Blaszczak E, Pantazopoulou M, Fischer B, Omnus DJ, Le Dez G, Brossard A, Gunnarsson A, Barry JD, Meurer M, *et al.* (2014). Protein quality control at the inner nuclear membrane. Nature 516, 410–413.
Klaips CL, Jayaraj GG, Hartl FU (2018). Pathways of cellular proteostasis in aging and disease. J Cell Biol 217, 51–63.
Kohlmann S, Schäfer A, Wolf DH (2008). Ubiquitin ligase Hul5 is required for fragment-specific substrate degradation in endoplasmic reticulum-associated degradation. J Biol Chem 283, 16374–16383.
Kriegenburg F, Jakopec V, Poulsen EG, Nielsen SV, Roguev A, Krogan N, Gordon C, Fleig U, Hartmann-Petersen R (2014). A chaperone-assisted degradation pathway targets kinetochore proteins to nsure genome stability. PLoS Genet 10, e1004140.
Land H, Humble MS (2018). YASARA: A tool to obtain structural guidance in biocatalytic investigations. Methods Mol Biol 2018;1685, 43–67.
Lee JW, Beebe K, Nangle LA, Jang J, Longo-Guess CM, Cook SA, Davisson MT, Sundberg JP, Schimmel P, Ackerman SL (2006). Editing-defective tRNA synthetase causes protein misfolding and neurodegeneration. Nature 443, 50–55.
Leggett DS, Hanna J, Borodovsky A, Crosas B, Schmidt M, Baker RT, Walz T, Ploegh H, Finley D (2002). Multiple associated proteins regulate proteasome structure and function. Mol Cell 10, 495–507.
Leidenheimer NJ, Ryder KG (2014). Pharmacological chaperoning: A primer on mechanism and pharmacology. Pharmacol Res 83, 10–19.
Levdikov VM, Barynin VV, Grebenko AI, Melik-Adamyan WR, Lamzin VS, Wilson KS (1998). The structure of SAICAR synthase: An enzyme in the de novo pathway of purine nucleotide biosynthesis. Structure 6, 363–376.
Matreyek KA, Starita LM, Stephany JJ, Martin B, Chiasson MA, Gray VE, Kircher M, Khechaduri A, Dines JN, Hause RJ, *et al.* (2018). Multiplex assessment of protein variant abundance by massively parallel sequencing. Nat Gen 50, 874–882.
Maurer MJ, Spear ED, Yu AT, Lee EJ, Shahzad S, Michaelis S (2016). Degradation signals for ubiquitin-proteasome dependent cytosolic protein quality control (CytoQC) in yeast. G3 6, 1853–1866.

McClellan AJ, Scott MD, Frydman J (2005). Folding and quality control of the VHL tumor suppressor proceed through distinct chaperone pathways. Cell 121, 739–748.
Mordret E, Dahan O, Asraf O, Rak R, Yehonadav A, Barnabas GD, Cox J, Geiger T, Lindner AB, Pilpel Y (2019). Systematic detection of amino acid substitutions in proteomes reveals mechanistic basis of ribosome errors and selection for translation fidelity. Mol Cell 75, 427–441.e5.
Morello JP, Salahpour A, Laperrière A, Bernier V, Arthus MF, Lonergan M, Petäjä-Repo U, Angers S, Morin D, Bichet DG, *et al.* (2000). Pharmacological chaperones rescue cell-surface expression and function of misfolded V2 vasopressin receptor mutants. J Clin Invest 105, 887–895.
Muhlrad D, Hunter R, Parker R (1992). A rapid method for localized mutagenesis of yeast genes. Yeast 8, 79–82.
Murata S, Minami Y, Minami M, Chiba T, Tanaka K (2001). CHIP is a chaperone-dependent E3 ligase that ubiquitylates unfolded protein. EMBO Rep 2, 1133–1138.
Murray BP, Correia MA (2001). Ubiquitin-dependent 26S proteasomal pathway: A role in the degradation of native human liver CYP3A4 expressed in Saccharomyces cerevisiae? Arch Biochem and Biophys 393, 106–116.
Nakatsukasa K, Huyer G, Michaelis S, Brodsky JL (2008). Dissecting the ER-associated degradation of a misfolded polytopic membrane protein. Cell 132, 101–112.
Neklesa TK, Tae HS, Schneekloth AR, Stulberg MJ, Corson TW, Sundberg TB, Raina K, Holley SA, Crews CM (2011). Small-molecule hydrophobic tagging-induced degradation of HaloTag fusion proteins. Nat Chem Biol 7, 538–543.
Niekamp JM, Evans MD, Scott AR, Smaldino PJ, Rubenstein EM (2019). TOM1 confers resistance to the aminoglycoside hygromycin B in Saccharomyces cerevisiae. MicroPubl Biol 2019, 10–13.
Nielsen SV, Stein A, Dinitzen AB, Papaleo E, Tatham MH, Poulsen EG, Kassem MM, Rasmussen LJ, Lindorff-Larsen K, Hartmann-Petersen R (2017). Predicting the impact of Lynch syndrome-causing missense mutations from structural calculations. PLoS Genet 13, 1–26.
Nillegoda NB, Theodoraki MA, Mandal AK, Mayo KJ, Ren HY, Sultana R, Wu K, Johnson J, Cyr DM, Caplan AJ (2010). Ubr1 and Ubr2 function in a quality control pathway for degradation of unfolded cytosolic proteins. Mol Biol Cell 21, 2102–2116.
Nishikawa SI, Fewell SW, Kato Y, Brodsky JL, Endo T (2001). Molecular chaperones in the yeast endoplasmic reticulum maintain the solubil- ity of proteins for retrotranslocation and degradation. J Cell Biol 153, 1061–1070
Padovani C, Jevtić P, Rapé M (2022). Quality control of protein complex composition. Mol Cell 82, 1439–1450.
Pedemonte N, Bertozzi F, Caci E, Sorana F, Di Fruscia P, Tomati V, Ferrera L, Rodríguez-Gimeno A, Berti F, Pesce E, *et al.* (2020). Discovery of a picomolar potency pharmacological corrector of the mutant CFTR chloride channel. Sci Adv 6, 1–14.
Pettersen EF, Goddard TD, Huang CC, Couch GS, Greenblatt DM, Meng EC, Ferrin TE (2004) UCSF Chimera–a visualization system for exploratory research and analysis. J Comput Chem 25, 1605–1612.
Pike AC, Brzozowski AM, Walton J, Hubbard RE, Thorsell AG, Li YL, Gustafsson JA, Carlquist M (2001). Structural insights into the mode of action of a pure antiestrogen. Structure 9, 145–153.
Pla-Prats C, Thomä NH (2022). Quality control of protein complex assembly by the ubiquitin–proteasome system. Trends Cell Biol 32, 696–706.
Plemper RK, Egner R, Kuchler K, Wolf DH (1998). Endoplasmic reticulum degradation of a mutated ATP-binding cassette transporter Pdr5 proceeds in a concerted action of Sec61 and the proteasome. J Biol Chem 273, 32848–32856.
Ravid T, Kreft SG, Hochstrasser M (2006). Membrane and soluble substrates of the Doa10 ubiquitin ligase are degraded by distinct pathways. EMBO J 25, 533–543.
Redler RL, Das J, Diaz JR, Dokholyan NV (2016). Protein destabilization as a common factor in diverse inherited disorders. J Mol Evol 82, 11–16.
Roman H (1956) A system selective for mutations affecting the synthesis of adenine in yeast. Compt Rend Trav Lab Carlsberg, Ser Physiol 26, 299–314.
Rosenbaum JC, Fredrickson EK, Oeser ML, Garrett-Engele CM, Locke MN, Richardson LA, Nelson ZW, Hetrick ED, Milac TI, Gottschling DE, *et al.* (2011). Disorder targets misorder in nuclear quality control degradation: A disordered ubiquitin ligase directly recognizes its misfolded substrates. Mol Cell 41, 93–106.
Rowe SM, Verkman AS (2013) Cystic fibrosis transmembrane regulator correctors and potentiators. Cold Spring Harb Perspect Med 3, a009761.
Runnebohm AM, Evans MD, Richardson AE, Turk SM, Olesen JB, Smaldino PJ, Rubenstein EM (2020). Loss of protein quality control gene UBR1 sensitizes Saccharomyces cerevisiae to the aminoglycoside hygromycin B. Fine Focus 6, 76–83.
Sato BK, Schulz D, Do PH, Hampton RY (2009). Misfolded membrane proteins are specifically recognized by the transmembrane domain of the Hrd1p ubiquitin ligase. Mol Cell 34, 212–222.
Saunders PP, Broquist HP (1966). Saccharopine, an intermediate of the aminoadipic acid pathway of lysine biosynthesis. IV. Saccharopine dehydrogenase. J Biol Chem 241, 3435–3440.
Schmidheini T, Mosch HU, Evans JNS, Braus G (1990). Yeast allosteric chorismate mutase is locked in the activated state by a single amino acid substitution. Biochemistry 29, 3660–3668.
Schnappauf G, Krappmann S, Braus GH (1998). Tyrosine and tryptophan act through the same binding site at the dimer interface of yeast chorismate mutase. J Biol Chem 273, 17012–17017.
Schymkowitz J, Borg J, Stricher F, Nys R, Rousseau F, Serrano L (2005). The FoldX web server: An online force field. Nucleic Acids Res 33(SUPPL. 2), 382–388.
Shearer AG, Hampton RY (2004). Structural control of endoplasmic reticulum-associated degradation. Effect of chemical chaperones on 3-hydroxy-3-methylglutaryl-CoA reductase. J Biol Chem 279, 188–196.
Shearer AG, Hampton RY (2005). Lipid-mediated, reversible misfolding of a sterol-sensing domain protein. EMBO J 24, 149–159.
Singh A, Vashistha N, Heck J, Tang X, Wipf P, Brodsky JL, Hampton RY (2020). Direct involvement of Hsp70 ATP hydrolysis in Ubr1-dependent quality control. Mol Biol Cell 31, 2669-2686.
Skieterska K, Rondou P, Van Craenenbroeck K (2017). Regulation of G protein-coupled receptors by ubiquitination. Int J Mol Sci 18, 10–13.
Song BL, Javitt NB, DeBose-Boyd RA (2005). Insig-mediated degradation of HMG CoA reductase stimulated by lanosterol, an intermediate in the synthesis of cholesterol. Cell Metab 1, 179–189.
Stein A, Fowler DM, Hartmann-Petersen R, Lindorff-Larsen K (2019). Biophysical and mechanistic models for disease-causing protein variants. Trends Biochem Sci 44, 575–588.
Sträter N, Håkansson K, Schnappauf G, Braus G, Lipscomb WN (1996). Crystal structure of the T state of allosteric yeast chorismate mutase and comparison with the R State. Proc Natl Acad Sci US 93, 3330–3334.
Sun X, Gao H, Yang Y, He M, Wu Y, Song Y, Tong Y, Rao Y (2019). Protacs: Great opportunities for academia and industry. Signal Transduct Target Ther 4, 64.
Swanson R, Locher M, Hochstrasser M (2001). A conserved ubiquitin ligase of the nuclear envelope/endoplasmic reticulum that functions in both ER-associated and Mat α2 repressor degradation. Genes Dev 2, 2660–2674.
Takahashi M, Shimodaira H, Andreutti-Zaugg C, Iggo R, Kolodner RD, Ishioka C (2007). Functional analysis of human MLH1 variants using yeast and in vitro mismatch repair assays. Cancer Res 67, 4595–4604.
Tang Y, Hicks JB, Hilvert D (1991). In vivo catalysis of a metabolically essential reaction by an antibody. Proc Natl Acad Sci USA 88, 8784–8786.
Tapper AR, McKinney SL, Nashmi R, Schwarz J, Deshpande P, Labarca C, Whiteaker P, Marks MJ, Collins AC, Lester HA (2004). Nicotine activation of α4* receptors: Sufficient for reward, tolerance, and sensitization. Science 306, 1029–1032
van den Boomen DJH, Volkmar N, Lehner PJ (2020). Ubiquitin-mediated regulation of sterol homeostasis. Curr Opin Cell Biol 65(Ldl), 103–111.
Van Goor F, Hadida S, Grootenhuis PD, Burton B, Cao D, Neuberger T, Turnbull A, Singh A, Joubran J, Hazlewood A, *et al.* (2009). Rescue of CF airway epithelial cell function in vitro by a CFTR potentiator, VX-770. Proc Natl Acad Sci USA 106, 18825–18830.
Van Goor F, Hadida S, Grootenhuis PD, Burton B, Stack JH, Straley KS, Decker CJ, Miller M, McCartney J, Olson ER, *et al.* (2011). Correction of the F508del-CFTR protein processing defect in vitro by the investigational drug VX-809. Proc Natl Acad Sci USA 108, 18843–18848.
Vo MN, Terrey M, Lee JW, Roy B, Moresco JJ, Sun L, Fu H, Liu Q, Weber TG, Yates JR 3rd, *et al.* (2018). ANKRD16 prevents neuron loss caused by an editing-defective tRNA synthetase. Nature 557, 510–515.
Wang Z, Moult J (2001). SNPs, protein structure, and disease. Hum Mutat 17, 263–270.
Wangeline MA, Vashistha N, Hampton RY (2017). Proteostatic tactics in the strategy of sterol regulation. Annu Rev Cell Dev Biol 33, 467–489.
Wangeline MA, Hampton RY (2018). "Mallostery"—ligand-dependent protein misfolding enables physiological regulation by ERAD. J Biol Chem 293, 14937–14950.
Wangeline MA, Hampton RY (2021). An autonomous, but INSIG-modulated, role for the sterol sensing domain in mallostery-regulated ERAD of yeast HMG-CoA reductase. J Biol Chem 296, 100063.

Wilhovsky S, Gardner R, Hampton R (2000). HRD gene dependence of endoplasmic reticulum-associated degradation. Mol Biol Cell 11, 1697–1708.
Woodruff KA, Richards KA, Evans MD, Scott AR, Voas BM, Irelan CB, Olesen JB, Smaldino PJ, Rubenstein EM (2021). Inner Nuclear Membrane Asi Ubiquitin Ligase Catalytic Subunits Asi1p and Asi3p, but not Asi2p, confer resistance to aminoglycoside hygromycin B in Saccharomyces cerevisiae. MicroPubl Biol 2021, 2–6.
Wong TS, Roccatano D, Zacharias M, Schwaneberg U (2006). A statistical analysis of random mutagenesis methods used for directed protein evolution. J Mol Biol 355, 858–871.
Winzeler EA, Shoemaker DD, Astromoff A, Liang H, Anderson K, Andre B, Bangham R, Benito R, Boeke JD, Bussey H, *et al*. (1999) Functional characterization of the *S. cerevisiae* genome by gene deletion and parallel analysis. Science 285, 901–906.
Xue Y, Lipscomb WN, Graf R, Schnappauf G, Braus G (1994). The crystal structure of allosteric chorismate mutase at 2.2-Å resolution. Proc Natl Acad Sci USA 91, 10814–10818.
Yagita Y, Zavodszky E, Peak-Chew SY, Hegde RS (2023). Mechanism of orphan subunit recognition during assembly quality control. Cell 186, 3443–3459.e24.
Yue P, Li Z, Moult J (2005). Loss of protein structure stability as a major causative factor in monogenic disease. J Mol Biol 353, 459–473.
Zelcer N, Sharpe LJ, Loregger A, Kristiana I, Cook EC, Phan L, Stevenson J, Brown AJ (2014). The E3 ubiquitin ligase MARCH6 degrades squalene monooxygenase and affects 3-Hydroxy-3-Methyl-Glutaryl Coenzyme A reductase and the cholesterol synthesis pathway. Mol Cell Biol 34, 1262–1270.
Zhao Y, MacGurn JA, Liu M, Emr S (2013). The ART-Rsp5 ubiquitin ligase network comprises a plasma membrane quality control system that protects yeast cells from proteotoxic stress. eLife 2013, 1–18.
Zheng N, Shabek N (2017). Ubiquitin Ligases: Structure, Function, and Regulation. Annu Rev Biochem 86, 129–157.
Zhu CC, Wojcikiewicz RJH (2000). Ligand binding directly stimulates ubiquitination of the inositol 1,4,5-trisphosphate receptor. Biochem J 348, 551–556.